Zolpidem restores sleep and slows Alzheimer's progression in a mouse model

Lu Yu[1,2], Shinya Yokomizo[1], Tri H.Doan[1], Qiuchen Zhao[1], Akshatha Ganne[3], Meenakshisundaram Balasubramaniam[3] , Ksenia V. Kastanenka[1 *]

1 Department of Neurology, MassGeneral Institute of Neurodegenerative Diseases, Mass General Brigham and Harvard Medical School, 114 16th Street, Charlestown, MA 02129, USA.

2 Department of Neurology, The Affiliated Hospital of Xuzhou Medical University, Xuzhou Medical University, Yunlong District, Xuzhou, 223006, China.

3 Department of Geriatrics, University of Arkansas for Medical Sciences, 629 Jack Stephens Dr, Little Rock, AR, 72205, USA.

Correspondence

Ksenia V. Kastanenka, Massachusetts General Hospital and Harvard Medical School, 114 16th Street, Room 2900, Charlestown, MA 02129, USA. E-mail: kkastanenka@mgh.harvard.edu

STRUCTURED ABSTRACT

INTRODUCTION: Deficits in Non-Rapid Eye Movement (NREM) sleep facilitate Alzheimer's disease (AD) progression. Enhancing GABAergic signaling can restore sleep. Unbiased computational analysis identified zolpidem as high-affinity GABA receptor modulator facilitating chloride transport that could slow AD.

METHODS: Zolpidem's effects on sleep and Alzheimer's progression were evaluated in young APP/PS1 mice. Sleep was monitored with EEG/EMG telemetry. Widefield imaging with voltage-sensitive dyes was used to track sleep-dependent brain rhythms. Multiphoton microscopy allowed

assessments of amyloid plaque load and basal neuronal calcium levels. Behavioral assays were used to measure memory and cognitive function.

RESULTS: Zolpidem restored NREM sleep and rescued sleep-dependent brain rhythm, slow oscillation. Zolpidem administration reduced cortical amyloid plaque burden, mitigated neuronal calcium overload, and enhanced sleep-dependent memory consolidation without adverse effects on locomotion.

DISCUSSION: Zolpidem effectively slowed Alzheimer's progression in young APP/PS1 mice. This supports zolpidem's therapeutic promise as an intervention strategy at early stages of AD.

1. BACKGROUND

Alzheimer's disease (AD) is a progressive neurodegenerative disorder and the leading cause of dementia worldwide, affecting over 55 million people globally, a number expected to double by 2050 [1, 2]. It is clinically characterized by progressive cognitive decline and memory impairment. AD is pathologically characterized by the accumulation of amyloid-beta (Aβ) plaques and neurofibrillary tau tangles[3, 4].

Sleep impairments have emerged as a major modifiable risk factor for Alzheimer's disease. Numerous studies have demonstrated that sleep deprivation and poor sleep quality are associated with increased amyloid-beta accumulation and accelerated disease progression[5, 6]. These pathological changes are closely linked to disruptions in the sleep-wake cycle, particularly deficits in non-rapid eye movement (NREM) sleep[7]. AD patients exhibit significant alterations in sleep architecture, including reduced NREM sleep duration, fragmented sleep, and diminished restorative sleep quality[8, 9]. Among these changes, impairments in slow oscillation (0.5- 1 Hz),

43 a sleep-dependent brain rhythm and the hallmark electrophysiological signature of deep NREM
44 sleep, have gained increasing attention. Slow oscillation is a large-amplitude, low-frequency
45 cortical rhythm that organizes synchronized neuronal activity across widespread brain networks.
46 Each slow oscillation cycle consists of a down-state of relative neuronal silence and an up-state of
47 synchronous neuronal firing[10-12]. Down and up states alternate during slow wave activity. Slow
48 oscillation is important for restorative sleep, contributing to cognitive functions such as memory
49 consolidation and learning in healthy individuals[10, 13]. Slow oscillation supports the
50 homeostatic regulation of sleep, increasing in response to prolonged wakefulness and decreasing
51 throughout the sleep period. In addition, slow oscillation helps organize faster brain rhythms,
52 including sleep spindles and sharp-wave ripples, thereby enhancing the efficiency of neural
53 networks involved in executive functions and synaptic plasticity[14-16]. Our published work
54 showed that optogenetic rescue of slow waves slowed AD, while exacerbating slow wave deficits
55 facilitated AD in a mouse model[17, 18]. Therefore, therapeutic targeting of slow oscillation could
56 present a promising approach to slowing Alzheimer's progression.

57 Mechanistically, impaired inhibitory neurotransmission has been identified as a major contributor
58 to slow wave disruptions in young APP/PS1 (APP) mice, a mouse model of amyloidosis. Our
59 published studies demonstrated that enhancing GABAergic tone through exogenous GABA
60 administration restored slow oscillation in APP mice. However, pharmacological block of GABA
61 receptors disrupted slow oscillation in healthy mice[18]. Similar to Alzheimer's patients, young
62 APP mice exhibit deficits in NREM sleep and increases in wake durations. Optogenetic stimulation
63 of GABAergic interneurons in the anterior cortex effectively rescued sleep deficits and restored
64 slow oscillation in APP mice [19]. These findings emphasize the importance of inhibitory circuits

65 in maintaining healthy sleep rhythms and suggest that strategies aimed at enhancing inhibitory
66 neurotransmission could have therapeutic benefits at early stages of AD.

67 Based on these insights, we performed an unbiased computational screen that identified zolpidem
68 as high-affinity $GABA_A$ receptor modulator facilitating chloride transport that could slow AD. We
69 adopted a translational approach by testing zolpidem, an FDA-approved drug that enhances
70 $GABA_A$ receptor activity and promotes sleep. We systematically assessed the therapeutic potential
71 of zolpidem in APP mice using multiple complementary experimental techniques. We first used in
72 vivo voltage-sensitive dye imaging to directly visualize the acute effects of zolpidem on cortical
73 slow oscillation dynamics across different doses, identifying 30 mg/kg as the optimal
74 concentration for restoring slow oscillation. Wireless EEG/EMG telemetry was used to
75 demonstrate that zolpidem improved NREM sleep architecture, enhancing NREM sleep continuity
76 and stability while reducing sustained wakefulness. Importantly, chronic daily administration of
77 zolpidem for four weeks significantly lowered amyloid plaque burden and neuronal calcium
78 overload. Behavioral assessments revealed that zolpidem treatment selectively improved memory
79 consolidation without adversely affecting locomotor activity or working memory. Collectively, our
80 findings suggest that zolpidem, an FDA-approved agent, may serve as a promising therapeutic
81 approach to restore sleep-dependent brain rhythms and ameliorate key pathological features of
82 Alzheimer's disease.

83

84 **2. METHODS**

85 **2.1. Animals and Drug Administration**

86 Male and female APPswe/PS1dE9 transgenic mice (APP, MMRRC 34829-JAX) were used. All
87 mice were maintained under a 12:12 h light/dark cycle (7am lights on, 7pm lights off) with ad
88 libitum access to food and water. For acute treatment experiments, APP mice aged 3–6 months
89 were used to assess immediate effects of zolpidem on slow oscillation and sleep architecture, both
90 of which were impaired during these ages[18-20]. For chronic treatment experiments, APP mice
91 aged 7–9 months were used to evaluate the long-term impact of zolpidem on AD-related pathology,
92 such as plaques and neuronal calcium overload, which are evident at these ages. Also, 7-9 month
93 old APP mice were treated with zolpidem and followed with assessments of memory function,
94 which is impaired at these ages[21]. All procedures were approved by the Institutional Animal
95 Care and Use Committee (IACUC, protocol number 2012N000085) and conducted in accordance
96 with NIH and ARRIVE guidelines.

97

98 **2.2. Voltage-Sensitive Dye (VSD) Imaging**

99 To evaluate the acute effects of zolpidem on cortical slow oscillation, wide-field in vivo imaging
100 was performed using the voltage-sensitive dye RH2080. APP mice (3–6 months old) underwent
101 craniotomy (5mm diameter) centered over the somatosensory cortex under 1–2% isoflurane
102 anesthesia. RH2080 (1 mg/mL in PBS) was applied topically for 1 hour. After washing off excess
103 dye with PBS and sealing the craniotomy with a glass coverslip, imaging was performed using a
104 Hamamatsu ORCA-ER CCD camera (Hamamatsu Photonics) with a 630 ± 10 nm excitation filter
105 and a >665 nm long-pass emission filter. Images were acquired at 20 Hz using Imaging Workbench
106 software (INDEC Systems). A single dose of zolpidem (3,10, 30 mg/kg) or vehicle (0mg/kg) was
107 administered via intraperitoneal (i.p.) injection, followed with repeated imaging at 5min intervals

during the first 30 minutes post-injection, followed by longer intervals up to 120 minutes. 10% DMSO in PBS served as vehicle. Data were motion-corrected and spatially filtered before analysis. Slow oscillation power was extracted using temporal band-pass filtering (0.5–1 Hz) and quantified across the cortical field of view.

VSD image sequences were analyzed using ImageJ. For each recording, fluorescence changes were expressed as $\Delta F/F_0$, where F_0 represented the minimum fluorescence intensity within the image sequence and ΔF was the change in pixel intensity relative to F_0. Mean $\Delta F/F_0$ values were extracted from a manually defined region of interest (ROI) over the somatosensory cortex. To quantify oscillatory dynamics, Fourier transform analysis was performed in MATLAB, allowing calculation of oscillation power.

2.3. EEG/EMG Sleep Recordings

APP mice (3–6 months old) were surgically implanted with wireless EEG/EMG telemetry devices (HD-X02, Data Sciences International, Minneapolis, MN) under isoflurane anesthesia (3% induction, 1.5% maintenance) using aseptic techniques. Telemetry transmitters were placed subcutaneously along the dorsum. The skull was exposed and cleaned, and two stainless steel screws (M06-15-M-SS-P, US Micro Screw) serving as EEG electrodes were secured through the skull to contact the dura. The anterior electrode was placed 1 mm anterior to bregma and 1 mm lateral to the midline, while the posterior electrode was positioned 3 mm posterior to bregma and 3 mm contralateral to the anterior screw. EMG leads were sutured into the bilateral nuchal muscles. Following surgery, mice were allowed to recover for 10 days before recordings began. EEG/EMG signals were acquired using Ponemah Software v6.50 (DSI) and continuously recorded while

130 animals were housed in individual home cages over receiver plates (RPC-1, DSI). Signals were
131 digitized with a bandwidth of 0.1–200 Hz and sampled at 500 Hz. EEG/EMG data, activity, and
132 temperature were recorded for 24 hours at baseline and for 48 hours following zolpidem (30 mg/kg,
133 i.p.) or vehicle injection.

134 Sleep scoring was performed using NeuroScore Software v3.6 (DSI), which allowed fully
135 automated sleep scoring to minimize experimenter bias as follows. Raw EEG and EMG signals
136 were imported and bandpass filtered (EEG: 0.5–100 Hz; EMG: 10–100 Hz). Data were segmented
137 into 10-second epochs and classified as wake, NREM sleep, or REM sleep using the integrated
138 Mouse Sleep Scoring module. Wakefulness was defined by high-frequency, variable EEG activity
139 and high EMG tone. NREM sleep was characterized by low-frequency, high-amplitude EEG and
140 low EMG tone. REM sleep was identified by dominance of theta-band activity (theta/delta power
141 ratio >3) and minimal EMG tone. Sleep bouts were defined as a minimum of two consecutive
142 epochs of the same state. Power spectral density analysis was performed using fast Fourier
143 transform (FFT) with a Hanning window applied to artifact-free epochs. Spectral bands were
144 defined as follows: slow oscillation (0.5–1 Hz), delta (1–4 Hz), theta (4–8 Hz), alpha (8–12 Hz),
145 sigma (12–16 Hz), and beta (16–24 Hz). Relative band power was computed as the ratio of
146 individual band power to total power. Changes in sleep architecture and spectral composition were
147 assessed across baseline and post-treatment periods.

148

149 **2.4. Multiphoton Imaging of Amyloid and Calcium**

150 To monitor AD-related pathology in vivo, we performed longitudinal two-photon imaging of
151 amyloid plaques and neuritic calcium using Methoxy-X04 and the genetically encoded ratiometric
152 calcium indicator Yellow Cameleon 3.6 (YC3.6) [22].

153

154 **2.4.1. AAV-YC3.6 Viral Injection**

155 Mice were initially anesthetized with 5% isoflurane in oxygen and maintained at 1.5% isoflurane
156 throughout the surgical procedure. Body temperature was maintained at approximately 37.5 °C
157 using a heating pad, and ophthalmic ointment was applied to protect the eyes. Using sterile
158 techniques, a 5 mm diameter round craniotomy was performed over the somatosensory cortex,
159 alternating between the right and left hemispheres across animals to minimize lateralization bias.

160 To visualize basal neuronal calcium levels, AAV2-CBA-YC3.6 (2 μL, 2×10^{12} vg/mL; University
161 of Pennsylvania Vector Core) was injected bilaterally into the posterior somatosensory cortices of
162 7-month-old APP mice. Stereotaxic coordinates relative to bregma were: AP −1.5 mm, ML
163 ±1.5 mm, DV −0.8 mm. The virus was delivered at a rate of 0.15 μL/min via a pulled glass
164 micropipette, which was left in place for an additional 10 minutes post-injection to facilitate viral
165 diffusion. Following viral injection, a sterile glass coverslip was positioned over the craniotomy
166 and secured using dental cement to form a chronic cranial window. The skin was sutured around
167 the window margin. Mice were allowed to recover on a heating pad until fully awake and mobile
168 and were subsequently monitored daily. Experimental imaging began three weeks post-surgery to
169 ensure complete recovery and sufficient transgene expression.

170

171 **2.4.2. Multiphoton Imaging of Amyloid Plaques**

172 To visualize amyloid plaque pathology in vivo, two-photon imaging was performed through
173 chronic cranial windows in mice. One day prior to imaging, mice received an intraperitoneal
174 injection of Methoxy-X04 (10 mg/kg, Tocris), which binds to fibrillar amyloid and enables
175 fluorescence-based detection. Immediately before imaging, Texas Red dextran (70 kDa, 2.5% in
176 PBS; Thermo Fisher) was administered intravenously via the retro-orbital sinus to label the
177 cerebral vasculature and facilitate anatomical orientation. Imaging was conducted using a
178 FluoView FV1000MPE two-photon laser-scanning imaging system (Olympus) mounted on a
179 BX61WI upright microscope with a 25× long working distance water-immersion objective (NA =
180 1.05, Olympus). A mode-locked Ti:Sapphire laser (MaiTai, Spectra-Physics) was tuned to 800 nm
181 to excite Methoxy-X04. Images were acquired at 1× digital magnification, and Z-stacks were
182 collected at 5 μm intervals. Body temperature was maintained using a heated stage, and mice
183 remained under 0.5–1% isoflurane anesthesia during acquisition.

184

185 **2.4.3. Multiphoton Imaging of Calcium**

186 To acquire basal neuronal calcium levels in APP mice, imaging of ratiometric YC3.6-expressing
187 neuronal processes (neurites) was performed through the same cranial windows as imaging of
188 amyloid plaques. APP mice were injected with AAV2-CBA-YC3.6 into the somatosensory cortex
189 three weeks prior to imaging as described above (2.4.1). Imaging was performed on the same two-
190 photon system using a Ti: Sapphire laser tuned to 860 nm to excite YC3.6. Fluorescence signals
191 were separated using a 510 nm dichroic mirror and collected via PMTs set to detect CFP (380–480
192 nm) and YFP (500–540 nm). ROIs were selected based on morphology and expression clarity.

193 Digital magnification was set to 2×. To minimize photodamage, laser power was maintained below
194 30 mW. Z-stack images were acquired at 1 μm intervals. Ratiometric (YFP/CFP) images were
195 generated pixel-wise, and calcium-overloaded neurites were identified as those with mean
196 YFP/CFP ratios exceeding 1.79, indicating cytosolic calcium levels >235 nM.

197

198 #### 2.4.4. Image Analysis

199 Z-stacks were aligned to baseline using rigid-body registration (TurboReg, ImageJ). Methoxy-
200 X04–labeled amyloid plaques were segmented using intensity-based thresholding and
201 reconstructed in 3D using Imaris (Bitplane). Total plaque burden was quantified as the sum of all
202 segmented plaque volumes per field of view, and change over time was expressed as percent of
203 baseline.

204 YC3.6-expressing neurites were manually segmented, and pixel-wise ratiometric YFP/CFP images
205 were generated. For each animal, multiple neurites were sampled per imaging session. A neurite
206 was defined as having calcium overload if its mean YFP/CFP ratio exceeded 1.79, corresponding
207 to intracellular calcium levels >235 nM. The proportion of overloaded neurites was calculated per
208 mouse and used as the primary outcome measure of treatment efficacy.

209

210 ### 2.5. Behavioral Testing

211 #### 2.5.1. Open Field Test

212 Mice were individually placed in a 27 × 27 × 20 cm acrylic arena and allowed to explore freely
213 for 10 minutes. Locomotion was tracked via video recording and analyzed with EthoVision XT

software (Noldus). Total distance traveled, time spent in the center zone, and center entry frequency were quantified to evaluate locomotor activity and anxiety-like behavior.

2.5.2. Y-Maze Test

Each mouse was introduced to the center of a Y-maze (arm dimensions: 5 × 30 × 12 cm; arms arranged at 120° angles) for a 10-minute exploration period. An arm entry required all four limbs to cross into an arm. Spontaneous alternation (SA) percentage was calculated as SA% = [Number of triads / (Total entries − 2)] × 100, with a triad defined as consecutive entries into three different arms. The maze was disinfected with 70% ethanol between tests.

2.5.3. Fear Conditioning Test

Training took place in chambers (30 × 24 × 21 cm; MED-Associates) equipped with a stainless-steel grid floor and auditory stimulation system. Following a 2-minute habituation, mice received three tone-shock pairings (80 dB, 30 s tone; 0.6 mA shock during the final 2 s, co-terminating with the tone), separated by 210-second intervals. Training was conducted between 5:00 and 7:00 pm.

For contextual recall, mice were returned to the same chambers 24 hours later and observed for 3 minutes without tone or shock. One hour later, cued recall was assessed in a modified environment with altered floor and wall features. After 3 minutes of exploration, a 30-second tone was presented without shock. Freezing behavior was automatically analyzed using Video Freeze software (Med Associates Inc.). Chambers were sanitized with 70% ethanol between sessions.

235 **2.6. Computational methods**

236 **2.6.1. High-throughput virtual screening**

237 For protein-ligand docking analysis, 3D structure of intact $GABA_A$ receptor unit was retrieved
238 from PDB databank (https://www.rcsb.org/) with accession ID 6D6U[23]. FDA-approved drug
239 library was retrieved from DrugBank database (https://go.drugbank.com/). $GABA_A$ receptor
240 structure was prepared before docking analysis, using Protein Preparation Wizard from
241 Schrodinger Maestro SBDD suite. Since the retrieved structure has a bound ligand (flumazenil),
242 before screening, a short simulation for 100ns was conducted without any intact ligand, using
243 Desmond simulation package to relax the protein complex. Retrieved FDA-approved drug library
244 was prepared using LigPrep module from Schrodinger Maestro SBDD suite. For high-throughput
245 virtual screening, Glide algorithm from Schrodinger Maestro SBDD suite was used[24]. Docking
246 grid-box was generated based on the information from bound ligand (flumazenil) in the retrieved
247 PDB structure (6D6U). The first stage docking was conducted using standard precision mode,
248 followed by high-precision mode. For Gibbs binding free energy, MMGBSA method was used via
249 Schrodinger Prime module[24].

250

251 **2.6.2. Machine learning and Neural network analysis**

252 For predicting $GABA_A$ receptor agonists and antagonists via machine learning approach, known
253 $GABA_A$ receptor agonists and antagonists were retrieved from PubChem database as smiles format
254 and converted to SDF format using OpenBabel. Molecular descriptors (both 2D and 3D) for the
255 retrieved compounds were calculated using QikProp module from Schrodinger SBDD suite[25].

256 Machine learning and neural network analysis were performed using Orange data mining
257 software[26, 27].

258

259 **2.6.3. Molecular Dynamic Simulation**

260 Molecular Dynamic (MD) simulations were performed using Desmond simulation package [28,
261 29]. Protein-ligand complex was first prepared using Protein Preparation Wizard from Maestro
262 Visualizer. To mimic the physiological conditions, MD simulations of $GABA_A$ receptor::drug
263 complex were performed in a virtual lipid bilayer (cell membrane) system. $GABA_A$ receptor::drug
264 complex was placed in a POPC lipid bilayer system in such a way that the lipid bilayer covers the
265 transmembrane region of $GABA_A$ receptor. This $GABA_A$ receptor::drug complex with intact lipid
266 bilayer was then immersed in a triclinic simulation box containing Simple Point Charge (SPC)
267 water. Simulation system was filled with 0.15M NaCl, excluding the counterions added to
268 neutralize the system. After energy minimization (5000 steps) and equilibration (300ps), the whole
269 system was simulated for 200ns. Simulation trajectories were analyzed for movement of chloride
270 ions in and out of the membrane pore present at the M2 transmembrane region of $GABA_A$.

271

272 **2.7. Statistical Analysis**

273 Statistical analyses were performed using GraphPad Prism 9. Data were first tested for normality
274 (Shapiro–Wilk test). Depending on distribution, comparisons were made using parametric
275 (unpaired t-test, two-way ANOVA with Tukey's) or non-parametric (Mann–Whitney U test,
276 Kruskal–Wallis test followed by Dunn's multiple comparisons test). Results are presented as mean

277 ± SEM unless otherwise specified. P-values < 0.05 were considered statistically significant. All
278 analyses were conducted with the experimenter blinded to treatment group.

279

280 **3. RESULTS**

281 **3.1. Computational Modeling Identified Structural Dynamics of Ligand Binding to**
282 **$GABA_A$ Receptor**

283 Young APP mice exhibit NREM sleep deficits and impairments of slow oscillation due to deficits
284 in GABA and GABA receptor expression. Thus, we set out to perform an unbiased computational
285 screen to identify an FDA-approved compound that could potentiate $GABA_A$ signaling, rescue
286 sleep and slow AD.

287 To investigate the structural dynamics involved in ligand binding to the $GABA_A$ receptor, the
288 three-dimensional quaternary structure of the receptor was retrieved from the Protein Data Bank
289 (PDB). The structure comprises two α subunits, two β subunits, and one γ subunit. Structural
290 visualization revealed the presence of a membrane pore (M2) and the benzodiazepine (BZD)
291 binding site (Fig. 1A). The BZD binding site is located at the interface between the α and γ subunits
292 of the $GABA_A$ receptor (Fig. 1A). Since both $GABA_A$ receptor agonists and antagonists primarily
293 target the BZD binding region[23, 30], docking calculations were performed using known positive
294 allosteric modulators (PAMs), e.g., diazepam, and competitive antagonists, e.g., flumazenil (FYP)
295 as standard ligands targeting the BZD binding site. The term "agonist" here refers to PAMs that
296 enhance GABA inhibitory action. The term "antagonist" refers to competitive antagonists, drugs
297 that inhibit GABA inhibitory action. Docking results predicted binding affinities of -38.91

298 kcal/mol for diazepam and -27.56 kcal/mol for flumazenil at the BZD site (Supplementary Fig.
299 1A).

300 To further understand the dynamics of ligand binding, 200 ns atomistic molecular dynamics (MD)
301 simulations were performed on the docked complexes of the $GABA_A$ receptor bound to either
302 diazepam or flumazenil, with the receptor embedded in a virtual lipid membrane (Supplementary
303 Fig. 1B). Since the chloride transport through the M2 membrane pore is one of the key functional
304 properties of the $GABA_A$ receptor, the number of chloride ions passing through the M2 pore during
305 the simulations was analyzed. Diazepam facilitated chloride ion transport across the membrane
306 throughout the 200 ns simulation (Supplementary Fig. 1C). In contrast, flumazenil inhibited
307 chloride ion transport across the membrane when bound to the $GABA_A$ receptor (Supplementary
308 Fig. 1D).

309

310 **3.2. High-throughput Virtual Screening and Neural Network Predicted High-affinity**
311 **$GABA_A$ Receptor Modulators**

312 To identify drug molecules targeting the $GABA_A$ receptor as potentiators, we computationally
313 screened an FDA-approved drug library against the BZD-binding site, based on the docking
314 models as shown in Fig. 1B. The docking protocol was conducted in two stages. In Stage I, a high-
315 throughput (standard-precision) docking approach was used to screen approximately 2,300 FDA-
316 approved drugs against the $GABA_A$ receptor. Drug candidates were ranked based on docking
317 scores (Fig. 1B). Since both agonists and antagonists bind at the BZD-binding site, machine
318 learning (ML) and neural network models were employed to classify potential agonists among the
319 top-ranked compounds. For model training, we curated a dataset of 32 known $GABA_A$ receptor

agonists and 24 antagonists from public sources, including the PubChem database. Multiple ML algorithms were evaluated, including Support Vector Machine (SVM), Logistic Regression, Random Forest, and Neural Networks. Molecular descriptors (~277) were computed for all compounds, both training and unknown, using the Mordred tool. Model development, training, and predictions were conducted using Orange Data Mining.

Model performance was assessed via random sampling. Among the tested models, SVM and Neural Networks showed the highest prediction accuracies, with SVM achieving 75.3% accuracy (AUC: 80.3%) and the Neural Network model achieving 74.4% accuracy (AUC: 77.3%). Other models, including Logistic Regression, showed accuracies below 70% and were therefore excluded from further analysis. Model training was repeated multiple times to ensure robustness, with SVM and Neural Network consistently demonstrating strong predictive performance. Once trained, these models were used to predict the agonist/antagonist classification for the full set of 2,256 FDA-approved therapeutics during Stage I. To minimize false positives, only compounds predicted as agonists by both the SVM and Neural Network models were selected, yielding 311 candidates (Fig. 1C).

To further refine the predictions, the top 200 compounds (top 10% from Stage I) were subjected to Stage II screening using the Molecular Mechanics Generalized Born Solvent (MM-GBSA) method. Drug candidates were ranked based on estimated Gibbs free energy of binding (Fig. 1D). Using predictions from both machine learning (properties) and computational docking (binding affinity) estimates (Fig. 1E), as well as its hypnotic properties, Zolpidem was selected as the leading drug candidate for further investigation.

342 **3.3. MD Simulation Predicted Stability in Zolpidem's Binding to $GABA_A$ Receptor and**
343 **Facilitating Chloride Ion Transport**

344 Protein-ligand docking analysis of the $GABA_A$ receptor bound to target drug molecules identified
345 key amino acid residues involved in ligand recognition. Diazepam interacted with γPhe77,
346 α1Thr162, α1Ser204, and α1Ser206 (Supplementary Fig. 2A-B). Protein-ligand interaction
347 profiling of $GABA_A$ receptor bound to zolpidem showed similar interaction pattern at the BZD-
348 binding site when compared to diazepam (Fig. 1F).

349 To evaluate the binding stability of zolpidem and its potential to facilitate chloride ion transport
350 across the membrane, a 200 ns molecular dynamics (MD) simulation of the $GABA_A$ receptor–
351 zolpidem complex was performed, with the receptor embedded in a virtual lipid bilayer. Simulation
352 trajectories were analyzed to assess binding stability and the number of contacts between chloride
353 ions and the M2 transmembrane region (chloride pore) of the receptor. Zolpidem maintained stable
354 binding at the BZD site throughout the 200 ns simulation (Supplementary Fig. 3A).

355 Snapshots from simulation trajectories at different time points revealed that zolpidem binding
356 induced structural changes in the $GABA_A$ receptor, notably the formation of a membrane pore
357 (Supplementary Fig. 3B). In contrast, competitive antagonist flumazenil inhibited such membrane
358 pore formation during the 200 ns simulation (Supplementary Fig. 3C).

359 Since zolpidem induced a membrane pore formation, we next examined whether it could facilitate
360 chloride ion transport. Analysis of the simulation trajectories for the number of chloride ions
361 passing through M2 membrane showed that zolpidem facilitated chloride ion transport across the
362 membrane, with an increased number of chloride ions passing through the M2 membrane pore
363 over the course of the 200 ns simulation (Supplementary Fig. 4A, B). Visualization of chloride ion

364 trajectories indicated Cl^- ions traversed the virtual membrane from the cytoplasmic side to the
365 extracellular side, interacting with M2 transmembrane residues (Supplementary Fig. 4A). Thus, as
366 a result of unbiased computational screen, zolpidem emerged as a leading candidate potentiating
367 $GABA_A$ signaling. Zolpidem's effect on slow oscillation, sleep and Alzheimer's progression was
368 tested in a mouse model of amyloidosis, young APP mice.

369 **3.4. Zolpidem Restored Slow Oscillation in APP Mice**

370 APP mice exhibit slow oscillation of low power compared to that of nontransgenic littermate
371 controls [19]. To determine the extent to which zolpidem restores slow oscillation in APP mice,
372 we first recorded baseline cortical slow wave activity using voltage-sensitive dye (VSD) through
373 cranial windows via wide-field microscopy in vivo. Subsequently, zolpidem at three different
374 concentrations (3, 10, 30 mg/kg) or vehicle control (0 mg/kg) was administered intraperitoneally
375 (i.p.) to APP mice (Fig. 2A).

376 Given the rapid permeability of zolpidem across the blood-brain barrier [31, 32], recordings were
377 taken at 5-minute intervals within the first 30 minutes post-injection, and at longer intervals up to
378 120 minutes post-injection. We observed a gradual increase in slow oscillation power after
379 zolpidem administration, reaching a significant elevation relative to baseline at 10, 15, and 20
380 minutes with a 30 mg/kg dose. Subsequently, slow oscillation power gradually declined, returning
381 to baseline levels (Fig. 2C). Meanwhile, APP mice treated with vehicle control showed no
382 significant changes in slow oscillation power throughout the 120-minute recording period
383 following injection (Fig. 2B). When directly compared with vehicle-treated controls, APP mice
384 treated with 30 mg/kg zolpidem exhibited significantly enhanced slow oscillation power at 10, 15,
385 and 20 minutes post-injection. However, lower concentrations of zolpidem (3 and 10 mg/kg) did

386 not produce significant changes in slow oscillation power compared to baseline or the vehicle
387 group (Supplemental Fig. 5). Therefore, we selected 30 mg/kg zolpidem for subsequent
388 experiments.

389

390 **3.5. Zolpidem Ameliorated NREM Sleep Deficits in APP Mice**

391 APP mice spend less time in NREM sleep and more time Awake compared to nontransgenic
392 littermate controls at 6 months of age [19]. To determine whether zolpidem could rescue NREM
393 sleep deficits in APP mice, we surgically implanted wireless EEG/EMG probes and performed
394 recordings to monitor sleep architecture in freely moving animals (Fig. 3A). 3-6 month old APP
395 mice were randomly assigned into one of two groups: vehicle-treated controls or mice receiving
396 30 mg/kg zolpidem consecutively for 2 days. Baseline sleep patterns were recorded on Day 0 prior
397 to intervention. On Day 1 and Day 2, animals received one injection per day at around ZT2 (2
398 hours after lights-on, corresponding to 9 AM) (Fig. 3B, C). EEG/EMG recordings were taken for
399 2 days post-injection, on Day 3 and Day 4, to monitor the lasting effects of the drug.

400 Compared to vehicle-treated APP mice, zolpidem treatment significantly increased NREM sleep
401 duration and reduced wakefulness during the 24 hours (Fig. 3D, G). That effect was prevalent
402 during the light phase, when mice spent more time for NREM sleep (Fig. 3E, H). However, the
403 effect of zolpidem was absent during the dark phase when animals were more active (Fig. 3F, I).
404 This suggested short-lived effects of the drug and limited toxicity. Drug effects lasted through the
405 light phase and did not carry over into the active dark phase. The sleep-inducing effects of
406 zolpidem disappeared as early as Day 3, the day after the final injection, suggesting a short-lasting
407 impact of zolpidem on sleep architecture. No significant group differences were observed in REM

408 sleep across all time points (Supplemental Fig. 6A–C). These findings indicate that zolpidem can
409 restore NREM sleep deficits in APP mice and not interfere with the active periods.

410 3.6. Zolpidem Enhanced Slow Oscillation and Dynamically Modulated High-Frequency 411 Rhythms in APP Mice

412 Our published findings demonstrate that young APP mice exhibit reduced slow wave power (0.5-
413 1Hz) and elevated higher-frequency components during sleep, indicative of cortical
414 hyperexcitability, an aberration commonly observed in young amyloidosis models[19]. To further
415 investigate the spectral dynamics following zolpidem administration, we analyzed EEG power
416 within the first 6 hours after the drug was administered. This window captures the immediate
417 pharmacological effects of zolpidem during the period when mice are naturally more likely to
418 sleep. We performed Fourier transform analysis on EEG data acquired within the first 6 hours post-
419 injection. This allowed us to determine the drug effects on cortical oscillatory activity. As shown
420 in Fig. 4A and B, compared to their own baseline, zolpidem treatment significantly increased slow
421 oscillation (0.5-1 Hz) and delta (1-4 Hz) power during the first 2-3 hours post-injection. This
422 reflected enhanced low-frequency activity associated with deep NREM sleep. Vehicle-treated mice
423 showed no significant change from baseline at any time point. Moreover, direct comparisons
424 between groups revealed that the slow oscillation power was significantly higher in the zolpidem
425 group than in the vehicle group at 2 hours post-injection (Fig. 4A).

426 For higher-frequency bands, zolpidem significantly suppressed theta (4–8 Hz) during 1-3 hours
427 post-injection compared to baseline (Fig. 4C). Alpha (8–12 Hz) was suppressed 1, 3-6 hours post-
428 injection compared to baseline (Fig. 4D). Sigma (12–16 Hz) activity was suppressed 3-6 hours
429 post-injection relative to baseline (Fig. 4E). The vehicle group showed no significant changes from

430 baseline in these bands. Importantly, zolpidem-treated mice exhibited significantly lower power
431 than vehicle-treated mice at hours 1-3 for theta, hours 1, 3-6 for alpha, hour 6 for sigma ($p < 0.05$)
432 (Fig. 4C-D). Thus, zolpidem facilitated lower brain rhythms and effectively suppressed higher
433 rhythms. In contrast, beta (16–24 Hz) power transiently increased in the zolpidem group during
434 the first hour, relative to both baseline and vehicle controls ($p < 0.05$), but returned to baseline
435 thereafter (Fig. 4F). Together, these results indicate that zolpidem alters the spectral profile in APP
436 mice by promoting slow oscillatory activity while dynamically modulating higher-frequency
437 rhythms in a time-dependent manner.

438

439 **3.7. Chronic Zolpidem Treatment Suppressed Amyloid Deposition in APP Mice**

440 Building on the sleep-enhancing effects of acute zolpidem treatment, we next sought to examine
441 whether sustained treatment could affect Alzheimer's disease pathology. Given the causal link
442 between NREM sleep impairments and accelerated Aβ deposition[33], we assessed the impact of
443 chronic daily zolpidem administration at 30mg/kg on amyloid burden at baseline, Weeks 2 and 4
444 of a 4-week treatment period (Fig. 5A).

445 To visualize amyloid plaques in vivo over time, amyloid deposits were labeled with Methoxy-X04.
446 Plaques were visualized in anesthetized mice through cranial windows using multiphoton
447 microscopy. Baseline imaging (Fig. 5B, C) was performed before the start of treatment, followed
448 by repeated imaging of same animals at Weeks 2 (Fig. 5D, E) and 4 (Fig. 5F, G). Plaque burden
449 was comparable between groups at baseline. In vehicle-treated APP mice, plaque burden gradually
450 increased, with a significant elevation at Week 4 compared to baseline. In contrast, zolpidem-
451 treated mice exhibited a substantial reduction in plaque burden beginning at Week 2, which

452 continued to decline through Week 4. A significant difference in plaque burden between zolpidem-
453 and vehicle-treated mice was observed at Week 2 and became more pronounced by Week 4 (Fig.
454 5H). Thus, chronic zolpidem treatment effectively suppressed Aβ accumulations.

455

456 3.8. Chronic Zolpidem Treatment Reduced the Percentage of Neuronal Processes with 457 Calcium Overload in APP Mice

458 Calcium homeostasis is necessary for proper neuronal function. Neuronal calcium homeostasis is
459 impaired in APP mice. A subset of cortical neurons exhibits calcium overload, or significant
460 elevations in basal calcium, due to amyloid β-induced dysregulation, particularly within neurites,
461 or neuronal processes of APP mice [34, 35]. To evaluate whether chronic zolpidem treatment can
462 restore neuronal calcium homeostasis, we expressed the ratiometric calcium indicator Yellow
463 Cameleon 3.6 (YC3.6) in the cortex of APP mice. YC3.6 is a genetically encoded FRET-based
464 sensor containing YFP and CFP fluorophores. YC3.6 allows determination of real-time
465 intracellular calcium levels. Neurites were classified as overloaded when the YFP/CFP ratio
466 exceeded 1.79, corresponding to intracellular calcium concentrations greater than 235 nM, or two
467 standard deviations above the mean of neurites in nontransgenic controls [22].

468 Representative images show numerous, red-labeled neurites with calcium overload (yellow arrows)
469 in vehicle-treated mice at 2 and 4 weeks (Fig. 6A, C, E). However, zolpidem-treated mice showed
470 a marked reduction in overloaded neurites over the same time period (Fig. 6B, D, F). Histograms
471 of YFP/CFP ratio distributions showed a progressive increase in the percentage of calcium-
472 overloaded neurites in the vehicle-treated group over time (Fig. 6G, red box). However, zolpidem-
473 treated mice exhibited a gradual reduction in the percentage if overloaded neurites over the

474 treatment period (Fig. 6H, red box). Quantitative analysis demonstrated that the percentage of
475 neurites exhibiting calcium overload increased in vehicle-treated mice from baseline to Week 2
476 and increased further at Week 4. However, zolpidem treatment significantly reduced the percentage
477 of neurites with calcium overload by Week 4, compared to baseline and vehicle controls (Fig. 6I).
478 These findings suggest that chronic zolpidem treatment restored calcium homeostasis and
479 prevented calcium overload in neurites of APP mice, providing evidence for its potential
480 neuroprotective effects beyond sleep regulation.

481

482 **3.9. Chronic Zolpidem Treatment Improved Memory Consolidation in APP Mice**

483 To determine whether chronic zolpidem treatment alters cognitive function in APP mice, we
484 conducted a series of behavioral assays, including open field, Y-maze, and fear conditioning tests,
485 following 4 weeks of daily treatment with either 30 mg/kg zolpidem or vehicle. In the open field
486 test (Fig. 7A), zolpidem- and vehicle-treated mice exhibited comparable total distance traveled,
487 average velocity, and frequency of center entries (Fig. 7B–D), indicating no significant differences
488 in locomotor activity or anxiety-like behavior between groups. Similarly, no significant differences
489 were observed in spontaneous alternations in the Y-maze test (Fig. 7E, F), suggesting that zolpidem
490 treatment did not impact working memory in APP mice under these conditions.

491 We next assessed sleep-dependent memory consolidation using a classical fear conditioning
492 paradigm (Fig. 7G). During the acquisition phase, both groups exhibited increased freezing
493 behavior over time (Fig. 7H), indicating successful formation of fear memory. Then animals were
494 placed back into their home cages and allowed to consolidate fear memory during sleep. Twenty-
495 four hours later, contextual fear recall was tested by reintroducing mice to the original training

496 environment without any tone or shock. Zolpidem-treated mice demonstrated significantly higher
497 freezing levels during contextual recall compared to vehicle-treated mice (Fig. 7I), suggesting
498 improved memory consolidation. In contrast, no significant differences were observed between
499 groups during cued recall in a novel context (Fig. 7J). These results suggest that chronic zolpidem
500 administration selectively enhances contextual memory consolidation in APP mice without
501 affecting general locomotion or working memory performance.

502

503 **4. DISCUSSION**

504 The current work identified that therapeutic targeting of sleep can profoundly impact the course of
505 Alzheimer's disease (AD) progression. We evaluated whether pharmacologically enhancing sleep-
506 dependent brain rhythms using FDA-approved hypnotic zolpidem could restore cortical slow
507 oscillation, improve NREM sleep duration, and alleviate key molecular and functional deficits in
508 APP mice. Acute zolpidem administration markedly boosted slow oscillation power and enhanced
509 sleep continuity, while chronic daily treatment over four weeks reduced amyloid plaque burden,
510 normalization of neuronal calcium homeostasis, and improvements in memory consolidation
511 without adversely affecting locomotor or general cognitive functions. These results underscore the
512 therapeutic potential of pharmacologically restoring sleep-dependent brain rhythms to slow AD
513 progression.

514 NREM sleep plays a key role in memory consolidation and the progression of AD [7]. Early-stage
515 AD patients exhibit significant disruptions in NREM sleep, reduced slow-wave sleep, increased
516 sleep fragmentation, and altered sleep architecture, linked to accelerated cognitive decline and
517 worsening neuropathology [9, 36-38]. Among the core electrophysiological features of deep

518 NREM sleep, slow oscillation (0.5-1 Hz) is a fundamental sleep-dependent brain rhythm. These
519 large-amplitude, low-frequency cortical waves reflect highly synchronized neuronal activity,
520 consisting of alternating down-states of neuronal silence and up-states of synchronous firing [10-
521 12]. Slow oscillation is essential for memory consolidation [39], synaptic homeostasis [40], and
522 metabolic waste clearance [41]. Impairments appear early in AD, often before substantial plaque
523 deposition yet in the presence of oligomeric Aβ, suggesting a causal role in disease progression
524 [42-44]. Our published work demonstrated that slow oscillation is impaired in APP mice, with
525 cortical desynchronization, neuronal calcium overload, and accelerated amyloid pathology.
526 Optogenetic restoration of slow oscillation slowed the AD progression, whereas further disruption
527 worsened disease in APP mice [17, 18], indicating slow oscillation is a viable therapeutic target.

528 Deficits in inhibitory tone also contribute to slow wave disruptions during prodromal and early
529 AD [19]. Exogenous GABA restored slow oscillation in an AD mouse model, whereas
530 pharmacological blockade of $GABA_A$ and $GABA_B$ receptors disrupted slow oscillation in healthy
531 nontransgenic mice. Altered cortical inhibitory interneuron activity in APP mice further links
532 interneuron dysfunction to impaired rhythms [17]. Using an optogenetic, we reported that rhythmic
533 stimulation of GABAergic interneurons at the endogenous frequency of slow oscillation, 0.6 Hz,
534 was sufficient to restore slow waves and sleep in APP mice [19]. Most importantly it slowed
535 Alzheimer's progression in APP mice. While this methodological strategy established a causal
536 relationship between interneuron-dependent impairments in cortical slow wave activity and
537 Alzheimer's progression, its translational potential remained limited.

538 We therefore performed an unbiased computational screen to identify an FDA-approved
539 compound that could rescue sleep, potentiate sleep-dependent brain rhythms and slow Alzheimer's
540 progression. Computational modeling revealed zolpidem's strong and stable binding to the

541 $GABA_A$ receptor at the BZD site, with structural dynamics similar to diazepam. Molecular
542 dynamics simulations showed that zolpidem facilitated chloride ion transport across the membrane,
543 suggesting its ability to restore inhibitory tone. High-throughput docking and machine learning
544 screening of FDA-approved drugs further prioritized zolpidem based on predicted binding affinity
545 and potentiation of GABA signaling. These findings provided a mechanistic basis for testing
546 zolpidem's potential to rescue disrupted network activity in AD by enhancing GABAergic
547 signaling and restoring cortical slow oscillation. To enhance translational impact based on these
548 computational findings, we tested zolpidem, an FDA-approved $GABA_A$ receptor modulator.
549 Zolpidem is a proven hypnotic known to potentiate inhibition, promote sleep onset and maintain
550 sleep clinically [45, 46]. Beyond its hypnotic effects, emerging evidence suggests that zolpidem
551 has demonstrated beneficial neuromodulatory effects in various neurological disorders, including
552 stroke [47, 48], traumatic brain injury [49, 50], and Parkinson's disease [51, 52]. Although
553 zolpidem has been shown to improve sleep quality in Alzheimer's patients, its impact on slow
554 oscillation dynamics and related AD pathology has not been thoroughly tested. As an initial step,
555 we employed in vivo VSD imaging to directly assess the impact of different doses of zolpidem on
556 cortical slow oscillation dynamics in APP mice. We identified 30 mg/kg as the most effective dose
557 for enhancing slow oscillation power, which guided the design of our subsequent chronic treatment
558 experiments.

559 Having established an effective dose for enhancing cortical slow oscillation, we next investigated
560 whether zolpidem could alleviate the characteristic sleep disturbances observed in APP mice. Prior
561 studies have shown that APP mice display fragmented sleep architecture, with increased
562 wakefulness and reduced NREM sleep, particularly during the light phase, their typical rest period
563 mirroring the sleep abnormalities seen in Alzheimer's patients [19, 53, 54]. Using EEG/EMG

recordings, we found that acute administration of 30 mg/kg zolpidem significantly increased NREM sleep during the 24-hour recording period, specifically during the light phase. These effects were not observed in vehicle-treated mice. Zolpidem effects dissipated by the following day. In addition, zolpidem had little to no impact on sleep architecture during the dark phase, the animals' natural period of wakefulness, indicating that zolpidem selectively enhanced rest-phase sleep without disrupting activity during the dark phase.

Fourier transform analyses of EEG recordings revealed dynamic spectral changes induced by zolpidem treatment. Consistent with our previous findings of cortical hyperexcitability characterized by reduced slow-wave power and elevated higher-frequency rhythms in APP mice, zolpidem significantly increased slow oscillation (0.5–1 Hz) and delta (1–4 Hz) power within the initial hours post-injection. Conversely, zolpidem markedly suppressed higher-frequency rhythms, including theta (4–8 Hz), alpha (8–12 Hz), and sigma (12–16 Hz), while transiently elevating beta (16–24 Hz) activity in the first hour following administration. These spectral changes underscore zolpidem's capacity to restore cortical excitatory-inhibitory balance, promoting deep sleep-associated low-frequency rhythms and dynamically modulating aberrant high-frequency activities prevalent in AD. These findings align with prior studies showing that zolpidem enhances slow-wave power and suppresses high-frequency EEG components during NREM sleep. For instance, previous work has demonstrated that zolpidem increases slow-wave (0.5- 4 Hz) amplitude and power in rodents [55-57], corroborating the spectral changes observed in our APP mice. However, not all studies report consistent outcomes, some have observed reductions in SWA, likely due to differences in disease models, zolpidem dose, or the timing and duration of EEG analysis [58, 59].

To determine whether these acute effects could translate into longer-term benefits, we implemented a chronic dosing regimen in which APP mice received daily zolpidem injections for four weeks.

587 Longitudinal two-photon imaging of amyloid plaques demonstrated that chronic zolpidem
588 administration significantly suppressed amyloid deposition relative to vehicle-treated controls.
589 This finding aligns with published studies indicating that impaired sleep exacerbates amyloid
590 accumulation, whereas enhancing deep NREM sleep facilitates Aβ clearance [37, 60, 61].

591 In parallel, multiphoton calcium imaging revealed that chronic zolpidem treatment significantly
592 reduced the proportion of neurites exhibiting calcium overload, a marker of synaptic dysfunction
593 and neurotoxicity in AD [34, 35]. The observed decrease in the YFP/CFP ratios within neurites
594 among zolpidem-treated mice suggests improved intracellular calcium homeostasis, which is
595 typically disrupted by elevated amyloid-beta levels and associated cortical hyperexcitability [35].
596 Importantly, the normalization of neuronal calcium levels was evident as early as two weeks into
597 treatment and became even more pronounced by week four, indicating a progressive, cumulative
598 therapeutic effect.

599 Finally, to determine whether these neurophysiological improvements translated into functional
600 gains, we conducted a battery of behavioral assays. Zolpidem-treated APP mice displayed intact
601 locomotor function and healthy working memory, as indicated by open field and Y-maze
602 performance. Notably, these mice exhibited enhanced contextual fear memory consolidation,
603 suggesting that improved sleep and cortical network synchronization directly enhanced memory
604 consolidation.

605 Zolpidem is FDA-approved hypnotic known to potentiate inhibitory tone and effective at inducing
606 sleep in humans. Although previous studies have reported potential adverse effects of zolpidem
607 treatment, including cognitive impairment and increased risk of falls in older adults, these
608 outcomes appear to be dose-dependent and population-specific [62-64]. That is, these adverse
609 outcomes could be attributed to long-treatment durations at high doses that induce toxicity. Indeed,

610 zolpidem is routinely prescribed to elderly populations and has demonstrated a favorable safety
611 profile in short-term intervention studies[63]. Supporting this, a recent randomized, triple-blind,
612 placebo-controlled clinical trial found that zolpidem effectively decreased wakefulness and
613 increased sleep duration in Alzheimer's patients, with mild to no adverse events reported [65].
614 Other clinical and preclinical studies have similarly reported beneficial effects of chronic zolpidem
615 administration. For example, long-term treatment with zolpidem has been shown to improve
616 neurological function and promote behavioral recovery in stroke [47, 66]. In line with these
617 findings, we did not observe any notable adverse effects on locomotion in our study. Short-duration
618 treatment of 4 weeks at relatively low doses of 30mg/kg failed to elicit toxicity and adverse side-
619 effects in APP mice as reported in present study. This may be attributable to factors such as
620 differences in animal models, disease stage, dosing regimen, or treatment duration. Thus,
621 intermittent low-dose administration at early AD stages, when cortical circuits are hyperactive
622 from reduced inhibitory tone, may maximize benefit while minimizing sedation risk. Collectively,
623 these observations highlight the importance of optimizing therapeutic strategies to maximize
624 clinical benefit while minimizing potential risks.

REFERENCES

1. J. Culberson, J. Kopel, U. Sehar, and P. H. Reddy, Urgent Needs of Caregiving in Ageing Populations with Alzheimer's Disease and Other Chronic Conditions: Support Our Loved Ones. Ageing Research Reviews, 2023: p. 102001.

2. M. A. Deture and D. W. Dickson, *The neuropathological diagnosis of Alzheimer's disease*. Molecular Neurodegeneration, 2019. **14**(1): p. 32.

3. P. Scheltens, B. De Strooper, M. Kivipelto, H. Holstege, G. Chételat, C. E. Teunissen, J. Cummings, and W. M. Van Der Flier, *Alzheimer's disease*. Lancet, 2021. **397**(10284): p. 1577-1590.

4. E. Liu, Y. Zhang, and J.-Z. Wang, *Updates in Alzheimer's disease: from basic research to diagnosis and therapies*. Translational Neurodegeneration, 2024. **13**(1): p. 45.

5. P. T. Nguyen Ho, S. J. W. Hoepel, M. Rodriguez-Ayllon, A. I. Luik, M. W. Vernooij, and J. Neitzel, *Sleep, 24-Hour Activity Rhythms, and Subsequent Amyloid-β Pathology*. JAMA Neurology, 2024. **81**(8): p. 824-834.

6. E. N. Minakawa, K. Wada, and Y. Nagai, *Sleep Disturbance as a Potential Modifiable Risk Factor for Alzheimer's Disease*. International Journal of Molecular Sciences, 2019. **20**(4): p. 803.

7. M. M. Lim, J. R. Gerstner, and D. M. Holtzman, *The sleep-wake cycle and Alzheimer's disease: what do we know?* Neurodegener Dis Manag, 2014. **4**(5): p. 351-62.

8. Z. Zavecz, V. D. Shah, O. G. Murillo, R. Vallat, B. A. Mander, J. R. Winer, W. J. Jagust, and M. P. Walker, *NREM sleep as a novel protective cognitive reserve factor in the face of Alzheimer's disease pathology*. BMC Medicine, 2023. **21**(1): p. 156.

9. B. P. Lucey, A. Mccullough, E. C. Landsness, C. D. Toedebusch, J. S. Mcleland, A. M. Zaza, A. M. Fagan, L. Mccue, C. Xiong, J. C. Morris, T. L. S. Benzinger, and D. M. Holtzman, *Reduced non-rapid eye movement sleep is associated with tau pathology in early Alzheimer's disease*. Sci Transl Med, 2019. **11**(474).

10. M. Steriade, A. Nuñez, and F. Amzica, A novel slow (< 1 Hz) oscillation of neocortical neurons in vivo: depolarizing and hyperpolarizing components. J Neurosci, 1993. **13**(8): p. 3252-65.

11. M. Ruiz-Mejias, L. Ciria-Suarez, M. Mattia, and M. V. Sanchez-Vives, *Slow and fast rhythms generated in the cerebral cortex of the anesthetized mouse*. Journal of Neurophysiology, 2011. **106**(6): p. 2910-2921.

12. M. V. Sanchez-Vives and D. A. Mccormick, *Cellular and network mechanisms of rhythmic recurrent activity in neocortex*. Nat Neurosci, 2000. **3**(10): p. 1027-34.

13. M. J. Esfahani, S. Farboud, H.-V. V. Ngo, J. Schneider, F. D. Weber, L. M. Talamini, and M. Dresler, *Closed-loop auditory stimulation of sleep slow oscillations: Basic principles and best practices*. Neuroscience & Biobehavioral Reviews, 2023. **153**: p. 105379.

14. L. Marshall, H. Helgadóttir, M. Mölle, and J. Born, *Boosting slow oscillations during sleep potentiates memory*. Nature, 2006. **444**(7119): p. 610-613.

15. O. Melamed, O. Barak, G. Silberberg, H. Markram, and M. Tsodyks, *Slow oscillations in neural networks with facilitating synapses*. Journal of Computational Neuroscience, 2008. **25**(2): p. 308-316.

16. J. Zhang, P.-C. Chen, S. C. Mednick, and A. Tambini, *Slow Oscillations Modulate Functional Brain Changes Supporting Working Memory*. bioRxiv, 2024: p. 2024.05.14.594161.

17. K. V. Kastanenka, M. Calvo-Rodriguez, S. S. Hou, H. Zhou, S. Takeda, M. Arbel-Ornath, A. Lariviere, Y. F. Lee, A. Kim, J. M. Hawkes, R. Logan, D. Feng, X. Chen, S. N. Gomperts, and B. J. Bacskai, *Frequency-dependent exacerbation of Alzheimer's disease neuropathophysiology*. Scientific Reports, 2019. **9**(1): p. 8964.

18. K. V. Kastanenka, S. S. Hou, N. Shakerdge, R. Logan, D. Feng, S. Wegmann, V. Chopra, J. M. Hawkes, X. Chen, and B. J. Bacskai, *Optogenetic Restoration of Disrupted Slow Oscillations Halts Amyloid Deposition and Restores Calcium Homeostasis in an Animal Model of Alzheimer's Disease*. PLoS One, 2017. **12**(1): p. e0170275.

19. Q. Zhao, M. Maci, M. R. Miller, H. Zhou, F. Zhang, M. Algamal, Y. F. Lee, S. S. Hou, S. J. Perle, H. Le, A. N. Russ, E. H. Lo, D. Gerashchenko, S. N. Gomperts, B. J. Bacskai, and K. V. Kastanenka, *Sleep restoration by optogenetic targeting of GABAergic neurons reprograms microglia and ameliorates pathological phenotypes in an Alzheimer's disease model*. Mol Neurodegener, 2023. **18**(1): p. 93.

20. N. Cankar, N. Beschorner, A. Tsopanidou, F. L. Qvist, A. R. Colaço, M. Andersen, C. Kjaerby, C. Delle, M. Lambert, F. Mundt, P. Weikop, M. Jucker, M. Mann, N. H. Skotte, and M. Nedergaard, *Sleep deprivation leads to non-adaptive alterations in sleep microarchitecture and amyloid-β accumulation in a murine Alzheimer model*. Cell Rep, 2024. **43**(11): p. 114977.

21. Y. F. Lee, A. N. Russ, Q. Zhao, S. J. Perle, M. Maci, M. R. Miller, S. S. Hou, M. Algamal, Z. Zhao, H. Li, N. Gelwan, Z. Liu, S. N. Gomperts, A. Araque, E. Galea, B. J. Bacskai, and K. V. Kastanenka, *Optogenetic targeting of astrocytes restores slow brain rhythm function and slows Alzheimer's disease pathology*. Sci Rep, 2023. **13**(1): p. 13075.

22. M. R. Miller, Y. F. Lee, and K. V. Kastanenka, Calcium sensor Yellow Cameleon 3.6 as a tool to support the calcium hypothesis of Alzheimer's disease. Alzheimers Dement, 2023. **19**(9): p. 4196-4203.

23. S. Zhu, C. M. Noviello, J. Teng, R. M. Walsh, Jr., J. J. Kim, and R. E. Hibbs, *Structure of a human synaptic GABA(A) receptor*. Nature, 2018. **559**(7712): p. 67-72.

24. M. Balasubramaniam, J. Narasimhappagari, L. Liu, A. Ganne, S. Ayyadevara, R. Atluri, H. Ayyadevara, G. Caldwell, R. J. Shmookler Reis, S. W. Barger, and W. S. T. Griffin, *Rescue of*

ApoE4-related lysosomal autophagic failure in Alzheimer's disease by targeted small molecules. Commun Biol, 2024. **7**(1): p. 60.

25. A. Mohan, N. Rendine, M. K. S. Mohammed, A. Jeeva, H. F. Ji, and V. R. Talluri, Structure-based virtual screening, in silico docking, ADME properties prediction and molecular dynamics studies for the identification of potential inhibitors against SARS-CoV-2 M(pro). Mol Divers, 2022. **26**(3): p. 1645-1661.

26. M. Balasubramaniam, A. Ganne, N. Mainali, S. Pahal, S. Ayyadevara, and R. J. Shmookler Reis, Alzheimer's-specific brain amyloid interactome: Neural-network analysis of intra-aggregate crosslinking identifies novel drug targets. iScience, 2024. **27**(1): p. 108745.

27. M. Balasubramaniam, S. Ayyadevara, A. Ganne, S. Kakraba, N. R. Penthala, X. Du, P. A. Crooks, S. T. Griffin, and R. J. Shmookler Reis, *Aggregate Interactome Based on Protein Cross-linking Interfaces Predicts Drug Targets to Limit Aggregation in Neurodegenerative Diseases*. iScience, 2019. **20**: p. 248-264.

28. M. Balasubramaniam, N. Mainali, S. K. Bowroju, P. Atluri, N. R. Penthala, S. Ayyadevera, P. A. Crooks, and R. J. Shmookler Reis, *Structural modeling of GSK3β implicates the inactive (DFG-out) conformation as the target bound by TDZD analogs*. Sci Rep, 2020. **10**(1): p. 18326.

29. M. Balasubramaniam, P. A. Parcon, C. Bose, L. Liu, R. A. Jones, M. R. Farlow, R. E. Mrak, S. W. Barger, and W. S. T. Griffin, *Interleukin-1β drives NEDD8 nuclear-to-cytoplasmic translocation, fostering parkin activation via NEDD8 binding to the P-ubiquitin activating site*. J Neuroinflammation, 2019. **16**(1): p. 275.

30. J. J. Kim, A. Gharpure, J. Teng, Y. Zhuang, R. J. Howard, S. Zhu, C. M. Noviello, R. M. Walsh, Jr., E. Lindahl, and R. E. Hibbs, *Shared structural mechanisms of general anaesthetics and benzodiazepines*. Nature, 2020. **585**(7824): p. 303-308.

31. T. Trenque, P. Bustany, D. Lamiable, S. Legros, and H. Choisy, *Pharmacokinetics and brain distribution of zolpidem in the rat after acute and chronic administration*. J Pharm Pharmacol, 1994. **46**(7): p. 611-3.

32. D. Garrigou-Gadenne, J. T. Burke, A. Durand, H. Depoortere, J. P. Thénot, and P. L. Morselli, *Pharmacokinetics, brain distribution and pharmaco-electrocorticographic profile of zolpidem, a new hypnotic, in the rat*. J Pharmacol Exp Ther, 1989. **248**(3): p. 1283-8.

33. B. P. Lucey, T. J. Hicks, J. S. Mcleland, C. D. Toedebusch, J. Boyd, D. L. Elbert, B. W. Patterson, J. Baty, J. C. Morris, V. Ovod, K. G. Mawuenyega, and R. J. Bateman, *Effect of sleep on overnight cerebrospinal fluid amyloid β kinetics*. Ann Neurol, 2018. **83**(1): p. 197-204.

34. M. Calvo-Rodriguez, E. K. Kharitonova, and B. J. Bacskai, *Therapeutic Strategies to Target Calcium Dysregulation in Alzheimer's Disease*. Cells, 2020. **9**(11): p. 2513.

35. K. V. Kuchibhotla, S. T. Goldman, C. R. Lattarulo, H. Y. Wu, B. T. Hyman, and B. J. Bacskai, Abeta plaques lead to aberrant regulation of calcium homeostasis in vivo resulting in structural and functional disruption of neuronal networks. Neuron, 2008. **59**(2): p. 214-25.

735 36. B. A. Mander, J. R. Winer, and M. P. Walker, *Sleep and Human Aging*. Neuron, 2017.
736 **94**(1): p. 19-36.

737 37. Y. E. Ju, B. P. Lucey, and D. M. Holtzman, *Sleep and Alzheimer disease pathology--a*
738 *bidirectional relationship*. Nat Rev Neurol, 2014. **10**(2): p. 115-9.

739 38. J. R. Winer, B. A. Mander, R. F. Helfrich, A. Maass, T. M. Harrison, S. L. Baker, R. T.
740 Knight, W. J. Jagust, and M. P. Walker, *Sleep as a Potential Biomarker of Tau and β-Amyloid*
741 *Burden in the Human Brain*. J Neurosci, 2019. **39**(32): p. 6315-6324.

742 39. S. Diekelmann and J. Born, *The memory function of sleep*. Nature Reviews
743 Neuroscience, 2010. **11**(2): p. 114-126.

744 40. G. Tononi and C. Cirelli, Sleep and the price of plasticity: from synaptic and cellular
745 homeostasis to memory consolidation and integration. Neuron, 2014. **81**(1): p. 12-34.

746 41. L. Xie, H. Kang, Q. Xu, M. J. Chen, Y. Liao, M. Thiyagarajan, J. O'donnell, D. J.
747 Christensen, C. Nicholson, J. J. Iliff, T. Takano, R. Deane, and M. Nedergaard, *Sleep Drives*
748 *Metabolite Clearance from the Adult Brain*. Science, 2013. **342**(6156): p. 373-377.

749 42. Y. F. Lee, D. Gerashchenko, I. Timofeev, B. J. Bacskai, and K. V. Kastanenka, *Slow Wave*
750 *Sleep Is a Promising Intervention Target for Alzheimer's Disease*. Frontiers in Neuroscience,
751 2020. **Volume 14 - 2020**.

752 43. B. A. Mander, S. M. Marks, J. W. Vogel, V. Rao, B. Lu, J. M. Saletin, S. Ancoli-Israel, W.
753 J. Jagust, and M. P. Walker, *β-amyloid disrupts human NREM slow waves and related*
754 *hippocampus-dependent memory consolidation*. Nature Neuroscience, 2015. **18**(7): p.
755 1051-1057.

756 44. Y.-E. S. Ju, J. S. Mcleland, C. D. Toedebusch, C. Xiong, A. M. Fagan, S. P. Duntley, J. C.
757 Morris, and D. M. Holtzman, *Sleep Quality and Preclinical Alzheimer Disease*. JAMA
758 Neurology, 2013. **70**(5): p. 587-593.

759 45. A. N. Edinoff, N. Wu, Y. T. Ghaffar, R. Prejean, R. Gremillion, M. Cogburn, A. A. Chami,
760 A. M. Kaye, and A. D. Kaye, *Zolpidem: Efficacy and Side Effects for Insomnia*. Health Psychol
761 Res, 2021. **9**(1): p. 24927.

762 46. K. J. Holm and K. L. Goa, Zolpidem: an update of its pharmacology, therapeutic
763 efficacy and tolerability in the treatment of insomnia. Drugs, 2000. **59**(4): p. 865-89.

764 47. T. Hiu, Z. Farzampour, J. T. Paz, E. H. Wang, C. Badgely, A. Olson, K. D. Micheva, G.
765 Wang, R. Lemmens, K. V. Tran, Y. Nishiyama, X. Liang, S. A. Hamilton, N. O'rourke, S. J. Smith,
766 J. R. Huguenard, T. M. Bliss, and G. K. Steinberg, *Enhanced phasic GABA inhibition during the*
767 *repair phase of stroke: a novel therapeutic target*. Brain, 2016. **139**(Pt 2): p. 468-80.

768 48. S. D. Hall, N. Yamawaki, A. E. Fisher, R. P. Clauss, G. L. Woodhall, and I. M. Stanford,
769 GABA(A) alpha-1 subunit mediated desynchronization of elevated low frequency oscillations
770 alleviates specific dysfunction in stroke--a case report. Clin Neurophysiol, 2010. **121**(4): p.
771 549-55.

49. R. Singh, C. Mcdonald, K. Dawson, S. Lewis, A. M. Pringle, S. Smith, and B. Pentland, *Zolpidem in a minimally conscious state*. Brain Inj, 2008. **22**(1): p. 103-6.

50. J. Whyte and R. Myers, Incidence of clinically significant responses to zolpidem among patients with disorders of consciousness: a preliminary placebo controlled trial. Am J Phys Med Rehabil, 2009. **88**(5): p. 410-8.

51. H. Y. Huang, Y. T. Hsu, Y. C. Wu, S. M. Chiou, C. H. Kao, M. C. Tsai, and C. H. Tsai, Zolpidem improves neuropsychiatric symptoms and motor dysfunction in a patient with Parkinson's disease after deep brain stimulation. Acta Neurol Taiwan, 2012. **21**(2): p. 84-6.

52. J. Lavoisy and J. Marsac, *Zolpidem in Parkinson's disease*. The Lancet, 1997. **350**(9070): p. 74.

53. J.-E. Kang, M. M. Lim, R. J. Bateman, J. J. Lee, L. P. Smyth, J. R. Cirrito, N. Fujiki, S. Nishino, and D. M. Holtzman, *Amyloid-β Dynamics Are Regulated by Orexin and the Sleep-Wake Cycle*. Science, 2009. **326**(5955): p. 1005-1007.

54. J. H. Roh, Y. Huang, A. W. Bero, T. Kasten, F. R. Stewart, R. J. Bateman, and D. M. Holtzman, *Disruption of the Sleep-Wake Cycle and Diurnal Fluctuation of β-Amyloid in Mice with Alzheimer's Disease Pathology*. Science Translational Medicine, 2012. **4**(150): p. 150ra122-150ra122.

55. F. Kersanté, R. J. Purple, and M. W. Jones, The GABAA receptor modulator zolpidem augments hippocampal-prefrontal coupling during non-REM sleep. Neuropsychopharmacology, 2023. **48**(4): p. 594-604.

56. H. Y. Chen, T. B. Kuo, F. Z. Shaw, C. J. Lai, and C. C. Yang, *Sleep-related vagotonic effect of zolpidem in rats*. Psychopharmacology (Berl), 2005. **181**(2): p. 270-9.

57. J. A. Reeves-Darby, L. F. Berro, D. M. Platt, D. Rüedi-Bettschen, J. P. Shaffery, and J. K. Rowlett, Pharmaco-EEG analysis of ligands varying in selectivity for α1 subunit-containing GABA(A) receptors during the active phase in rats. Psychopharmacology (Berl), 2023. **240**(12): p. 2561-2571.

58. C. Kopp, U. Rudolph, and I. Tobler, *Sleep EEG changes after zolpidem in mice*. Neuroreport, 2004. **15**(14): p. 2299-302.

59. A. C. Fitzgerald, B. T. Wright, and S. A. Heldt, The behavioral pharmacology of zolpidem: evidence for the functional significance of α1-containing GABA(A) receptors. Psychopharmacology (Berl), 2014. **231**(9): p. 1865-96.

60. L. Xie, H. Kang, Q. Xu, M. J. Chen, Y. Liao, M. Thiyagarajan, J. O'donnell, D. J. Christensen, C. Nicholson, J. J. Iliff, T. Takano, R. Deane, and M. Nedergaard, *Sleep drives metabolite clearance from the adult brain*. Science, 2013. **342**(6156): p. 373-7.

61. J. E. Kang, M. M. Lim, R. J. Bateman, J. J. Lee, L. P. Smyth, J. R. Cirrito, N. Fujiki, S. Nishino, and D. M. Holtzman, *Amyloid-beta dynamics are regulated by orexin and the sleep-wake cycle*. Science, 2009. **326**(5955): p. 1005-7.

62. J. Glass, K. L. Lanctôt, N. Herrmann, B. A. Sproule, and U. E. Busto, *Sedative hypnotics in older people with insomnia: meta-analysis of risks and benefits*. Bmj, 2005. **331**(7526): p. 1169.

63. V. Scharner, L. Hasieber, A. Sönnichsen, and E. Mann, Efficacy and safety of Z-substances in the management of insomnia in older adults: a systematic review for the development of recommendations to reduce potentially inappropriate prescribing. BMC Geriatr, 2022. **22**(1): p. 87.

64. P. S. Wang, R. L. Bohn, R. J. Glynn, H. Mogun, and J. Avorn, *Zolpidem use and hip fractures in older people*. J Am Geriatr Soc, 2001. **49**(12): p. 1685-90.

65. L. L. Louzada, F. V. Machado, J. L. Quintas, G. A. Ribeiro, M. V. Silva, D. L. Mendonça-Silva, B. S. B. Gonçalves, O. T. Nóbrega, and E. F. Camargos, *The efficacy and safety of zolpidem and zopiclone to treat insomnia in Alzheimer's disease: a randomized, triple-blind, placebo-controlled trial*. Neuropsychopharmacology, 2022. **47**(2): p. 570-579.

66. Z.-G. Zhong, G.-J. Tao, S.-M. Hao, H. Ben, W.-M. Qu, F.-Y. Sun, Z.-L. Huang, and M.-H. Qiu, Alleviating sleep disturbances and modulating neuronal activity after ischemia: Evidence for the benefits of zolpidem in stroke recovery. CNS Neuroscience & Therapeutics, 2024. **30**(2): p. e14637.

ACKNOWLEDGEMENT

The works was supported by is made to the donors of Alzheimer's Disease Research, a program of BrightFocus Foundation, for support of this research (KVK, QZ).

CONFLICT OF INTEREST

The authors declare no conflicts of interest.

FUNDING SOURCES

This work was supported by National Institutes of Health Grant R01AG066171 (KVK), Cure Alzheimer's Fund (KVK), Chan Zuckerberg Initiative DAF Fund (Schultz, KVK). Overseas research fellowship, Japan Society for the Promotion of Science 202360054 (SY), Advanced Program of The Affiliated Hospital of Xuzhou Medical University PYJH2024314 (LY).

CONSENT STATEMENT

No human data was derived and, therefore, consent was not necessary.

KEYWORDS

Zolpidem; $GABA_A$ receptor; Slow oscillation; NREM sleep; Sleep; Alzheimer's disease; APP/PS1 mice; Amyloid plaques; Calcium homeostasis; Memory consolidation; Neurodegeneration

845 **LEGENDS**

846 **Figure 1. Quaternary structure and functional dynamics of the $GABA_A$ receptor. (A)**
847 Experimental structure of the $GABA_A$ receptor showing distinct subunits (colored based on
848 $GABA_A$ receptor subunits, BZD, α, β, and Y), forming the quaternary assembly. The ligand-
849 binding site, Benzodiazepine (BZD) binding site, is delineated with a box. **(B)** Predicted docking
850 scores for the FDA-approved drug library, ranked from highest to lowest interaction energies
851 during Stage I of the screen. **(C)** Machine learning and neural network-based classification of the
852 top 300 compounds from (**B**), distinguishing predicted $GABA_A$ receptor agonists from antagonists.
853 (**D**) Predicted Molecular Mechanics-Generalized Born Solvent Accessible (MM-GBSA)-based
854 Gibbs binding free energies for the top 200 compounds identified in (B) during Stage I of the
855 screen. **(E)** Comparison of predicted Gibbs binding free energies for zolpidem and eszopiclone
856 with that of diazepam. **(F)** Predicted binding pose of zolpidem in complex with the $GABA_A$
857 receptor, highlighting interacting residues within the BZD binding site.

858 **Figure 2. Voltage-sensitive dye (VSD) imaging revealed zolpidem-induced enhancement of**
859 **cortical slow oscillation. (A)** Schematic of VSD imaging setup over somatosensory cortex in an
860 APP mouse. **(B)** Statistical comparison of slow oscillation (0.5–1 Hz) power before and after
861 vehicle (0 mg/kg) treatment. Friedman test followed by Dunn's multiple comparisons test. **(C)**
862 Statistical comparison of slow oscillation (0.5–1 Hz) power before and after 30 mg/kg zolpidem
863 treatment. Friedman test followed by Dunn's multiple comparisons test. **(D)** Time course of
864 normalized slow oscillation power across 120 minutes post-gavage in vehicle (0 mg/kg), 10 mg/kg,
865 and 30 mg/kg treated groups. one-way ANOVA followed by Tukey's post hoc multiple
866 comparisons test. Data shown as mean ± SEM (n=5 mice/group). *$p < 0.05$, **$p < 0.01$. n.s., non-
867 significant. Lack of stars indicates lack of significance.

868

869 **Figure 3. Zolpidem acutely increased NREM sleep and reduced wakefulness in APP mice**. **(A)**
870 Experimental timeline for EEG/EMG recordings showing baseline, zolpidem administration on
871 days 1 and 2, and post-treatment recording on days 3 and 4. **(B)** Representative hypnogram, EEG
872 spectrogram, EEG/EMG traces, and locomotor activity for a vehicle-treated mouse. **(C)**
873 Corresponding plots for a zolpidem-treated mouse, demonstrating increased NREM sleep (blue)
874 and reduced wakefulness (yellow) during the light phase. **(D-F)** Quantification of NREM sleep
875 durations across 24 hours (**D**), light phase (**E**), and dark phase (**F**). **(G-I)** Quantification of
876 wakefulness durations across 24 hours (**G**), light phase (**H**), and dark phase (**I**). Mixed-effects
877 analysis followed by Tukey's multiple comparisons test. Black* indicates significant group
878 differences between zolpidem and vehicle treatments. Data shown as mean ± SEM (n=6-7
879 mice/group). *$p < 0.05$; **$p < 0.01$. Lack of stars indicates lack of significance.

880

881 Figure 4. Zolpidem dynamically modulated cortical oscillatory activity across multiple frequency
882 bands in APP mice during NREM sleep. We analyzed EEG power during NREM sleep within the
883 first 6 hours after the drug was administered and presented the hourly changes. (A) Slow oscillation
884 power (0.5–1 Hz) across treatment groups. (B) Delta power (1–4 Hz) across treatment groups. (C)
885 Theta power (4–8 Hz) across treatment groups. (D) Alpha power (8–12 Hz) across treatment
886 groups. (E) Sigma power (12–16 Hz) across treatment groups. (F) Beta power (16–24 Hz) across
887 treatment groups. Two-way ANOVA followed by Tukey's multiple comparisons test. Blue*
888 indicates significant differences compared to baseline within the zolpidem group. Black* indicates
889 significant group differences between zolpidem and vehicle treatments. Data shown as mean ±

890 SEM (n=6-7 mice/group). *p < 0.05; **p < 0.01; ***p < 0.001. Lack of stars indicates lack of
891 significance.

892

893 **Figure 5. Chronic zolpidem treatment reduced amyloid plaque burden in APP mice. (A)**
894 Experimental timeline of multiphoton imaging at baseline, 2 weeks, and 4 weeks of treatment. **(B-**
895 **G)** Representative two-photon images of amyloid plaques (cyan, Methoxy-X04 labeling) and
896 cortical vasculature (red, Texas Red dextran) at baseline (**B, C**), after 2 weeks of treatment (**D, E**),
897 and after 4 weeks of treatment (**F, G**) for vehicle (**B, D, F**) and zolpidem-treated mice (**C, E, G**).
898 Zolpidem treatment visibly reduced plaque accumulation over time. **(H)** Quantification of cortical
899 plaque burden over the 4-week treatment period. Zolpidem significantly reduced amyloid plaque
900 burden compared to both baseline and vehicle-treated controls. Mixed-effects analysis followed
901 by Tukey's multiple comparisons test. Blue* indicates significant differences compared to baseline
902 within the zolpidem group. Red* indicates significant differences compared to baseline within the
903 vehicle group. Black* indicates significant group differences between zolpidem and vehicle
904 treatments. Data shown as mean ± SEM (n=6-7 mice/group). *p < 0.05; **p < 0.01; ***p < 0.001.

905

906 **Figure 6. Zolpidem restored neuronal calcium homeostasis in APP mice. (A–F)** Representative
907 images of YC3.6-labeled neurites showing calcium overload (red) in vehicle and zolpidem groups
908 at baseline, 2 weeks, and 4 weeks. **(G–H)** Histograms of YFP/CFP ratios within neurite
909 populations treated with vehicle (**G**) and zolpidem (**H**). **(I)** Quantification of calcium-overloaded
910 neurites (%) across groups. Mixed-effects analysis followed by Tukey's multiple comparisons test.
911 Blue* indicates significant differences compared to baseline within the zolpidem group. Red*

912 indicates significant differences between the zolpidem group and vehicle group at the indicated
913 time point. Black* indicates significant group differences between zolpidem and vehicle
914 treatments. Data shown as mean ± SEM (n=6-7 mice/group). *$p < 0.05$; **$p < 0.01$; ***$p < 0.001$.

915

916 **Figure 7**. **Zolpidem improved contextual memory without affecting locomotor or working**
917 **memory. (A)** Experimental setup for open field. **(B–D)** Distance travelled (**B**), velocity (**C**) and
918 center entries (**D**) as a measure of open field performance across groups. (**E**) Experimental setup
919 for Y-maze test. **(F)** Y-maze alternation rates across groups. **(G)** Contextual fear conditioning setup.
920 **(H-J)** Fear acquisition (**H**), contextual recall (**I**) and cued recall (**J**) across groups. Unpaired two-
921 tailed t-test. Data shown as mean ± SEM (n=9-10 mice/group). *$p < 0.05$.

922

Figure 1

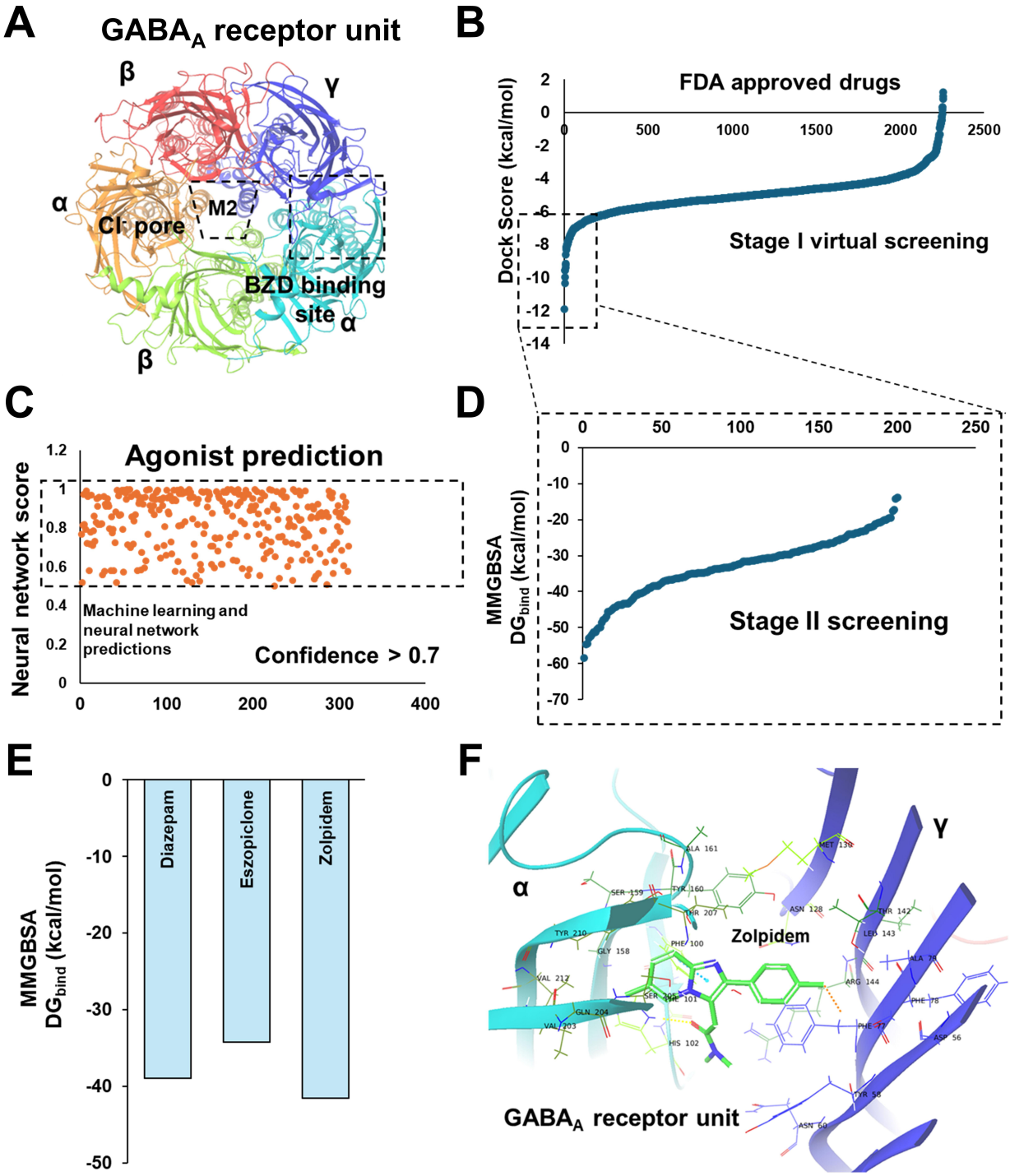
A
GABA$_A$ receptor unit
β
γ
α
M2
Cl⁻ pore
BZD binding site
α
β
B
FDA approved drugs
Dock Score (kcal/mol)
2
0
-2
-4
-6
-8
-10
-12
-14
0
500
1000
1500
2000
2500
Stage I virtual screening
C
Agonist prediction
Neural network score
1.2
1
0.8
0.6
0.4
0.2
0
Machine learning and neural network predictions
Confidence > 0.7
0
100
200
300
400
D
MMGBSA
DG$_{bind}$ (kcal/mol)
0
-10
-20
-30
-40
-50
-60
-70
0
50
100
150
200
250
Stage II screening
E
MMGBSA
DG$_{bind}$ (kcal/mol)
0
-10
-20
-30
-40
-50
Diazepam
Eszopiclone
Zolpidem
F
α
γ
Zolpidem
GABA$_A$ receptor unit

Figure 2

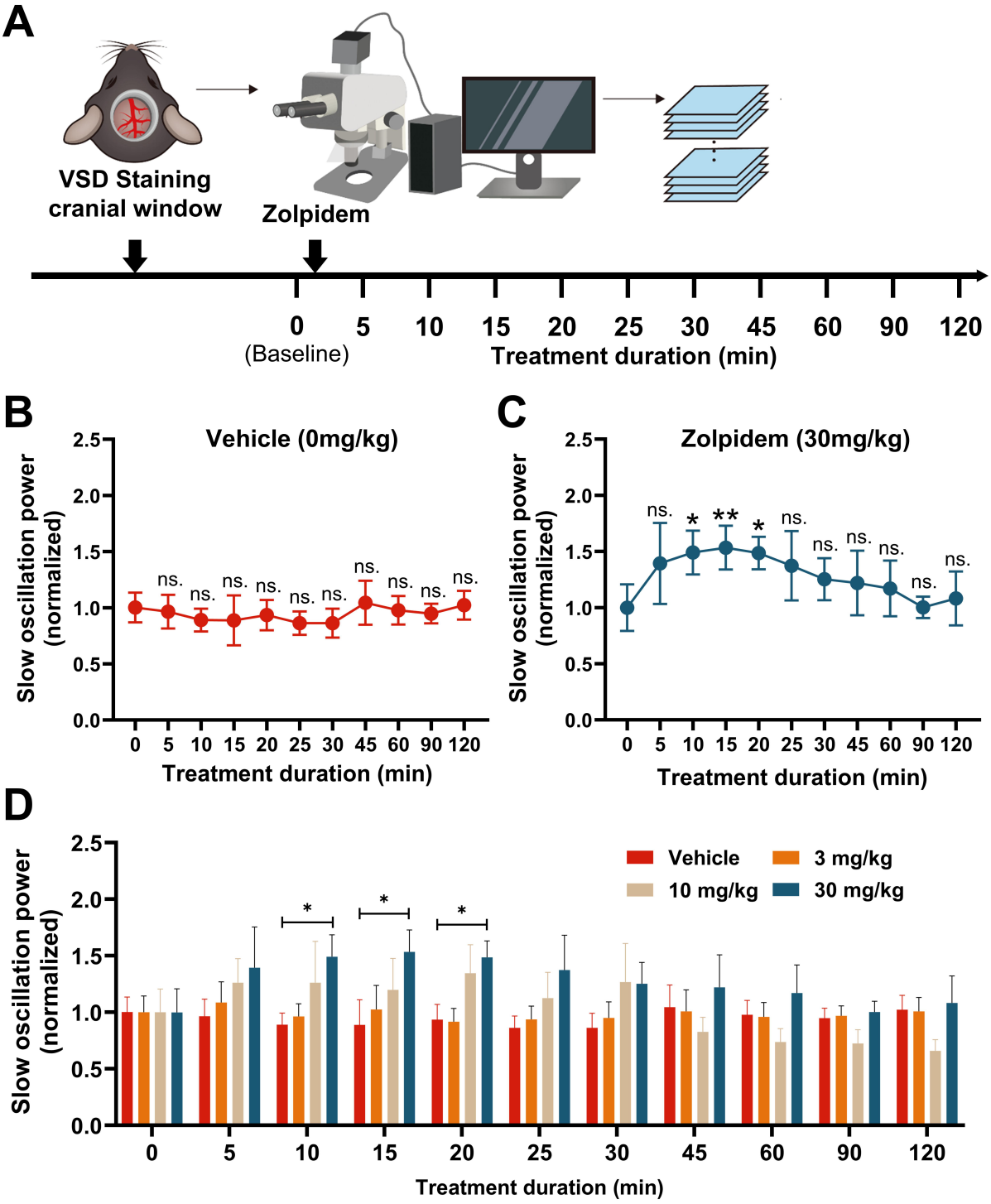
A
VSD Staining
cranial window
Zolpidem
0
(Baseline)
5
10
15
20
25
30
45
60
90
120
Treatment duration (min)
B
Vehicle (0mg/kg)
Slow oscillation power
(normalized)
2.5
2.0
1.5
1.0
0.5
0.0
ns.
Treatment duration (min)
C
Zolpidem (30mg/kg)
Slow oscillation power
(normalized)
ns.
*
**
*
ns.
Treatment duration (min)
D
Vehicle
3 mg/kg
10 mg/kg
30 mg/kg
Slow oscillation power
(normalized)
*
Treatment duration (min)

Figure 3

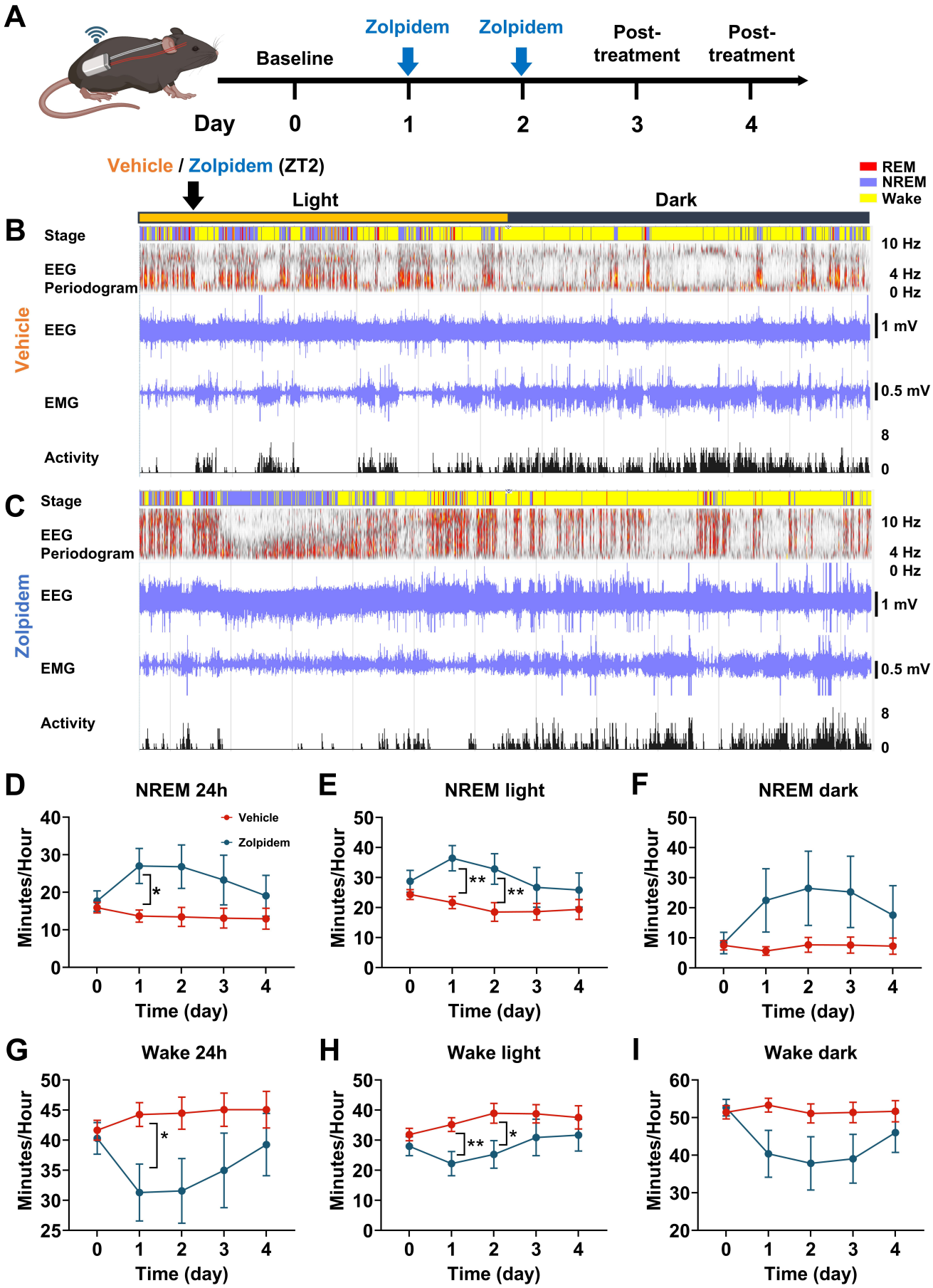
A
Zolpidem
Zolpidem
Baseline
Post-treatment
Post-treatment
Day
0
1
2
3
4
Vehicle / Zolpidem (ZT2)
REM
NREM
Wake
Light
Dark
B
Stage
EEG Periodogram
10 Hz
4 Hz
0 Hz
Vehicle
EEG
1 mV
EMG
0.5 mV
Activity
8
0
C
Stage
EEG Periodogram
10 Hz
4 Hz
0 Hz
Zolpidem
EEG
1 mV
EMG
0.5 mV
Activity
8
0
D
NREM 24h
Vehicle
Zolpidem
Minutes/Hour
Time (day)
E
NREM light
F
NREM dark
G
Wake 24h
H
Wake light
I
Wake dark

Figure 4

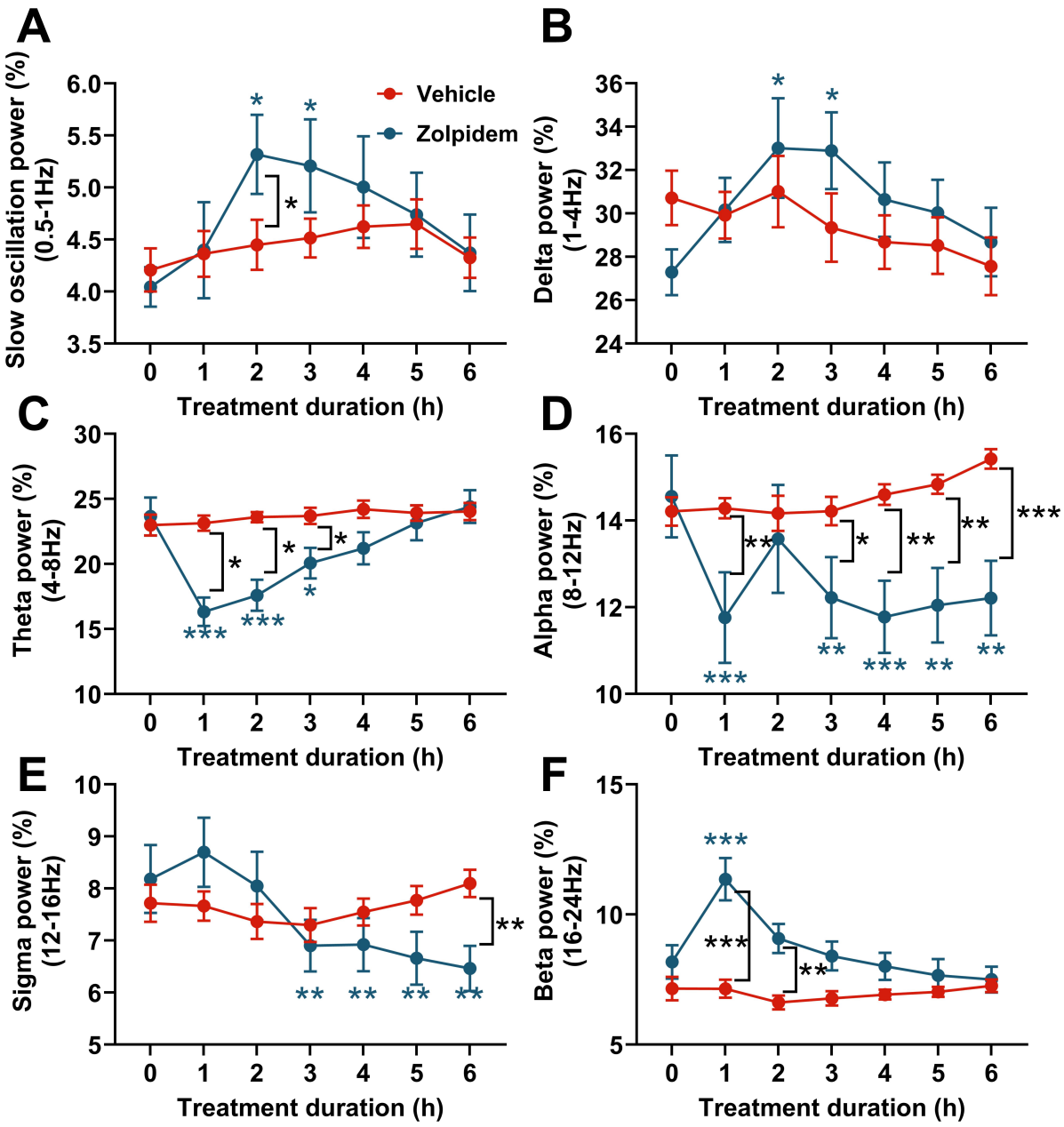
A
Slow oscillation power (%) (0.5-1Hz)
Vehicle
Zolpidem
Treatment duration (h)
B
Delta power (%) (1-4Hz)
Treatment duration (h)
C
Theta power (%) (4-8Hz)
Treatment duration (h)
D
Alpha power (%) (8-12Hz)
Treatment duration (h)
E
Sigma power (%) (12-16Hz)
Treatment duration (h)
F
Beta power (%) (16-24Hz)
Treatment duration (h)

Figure 5

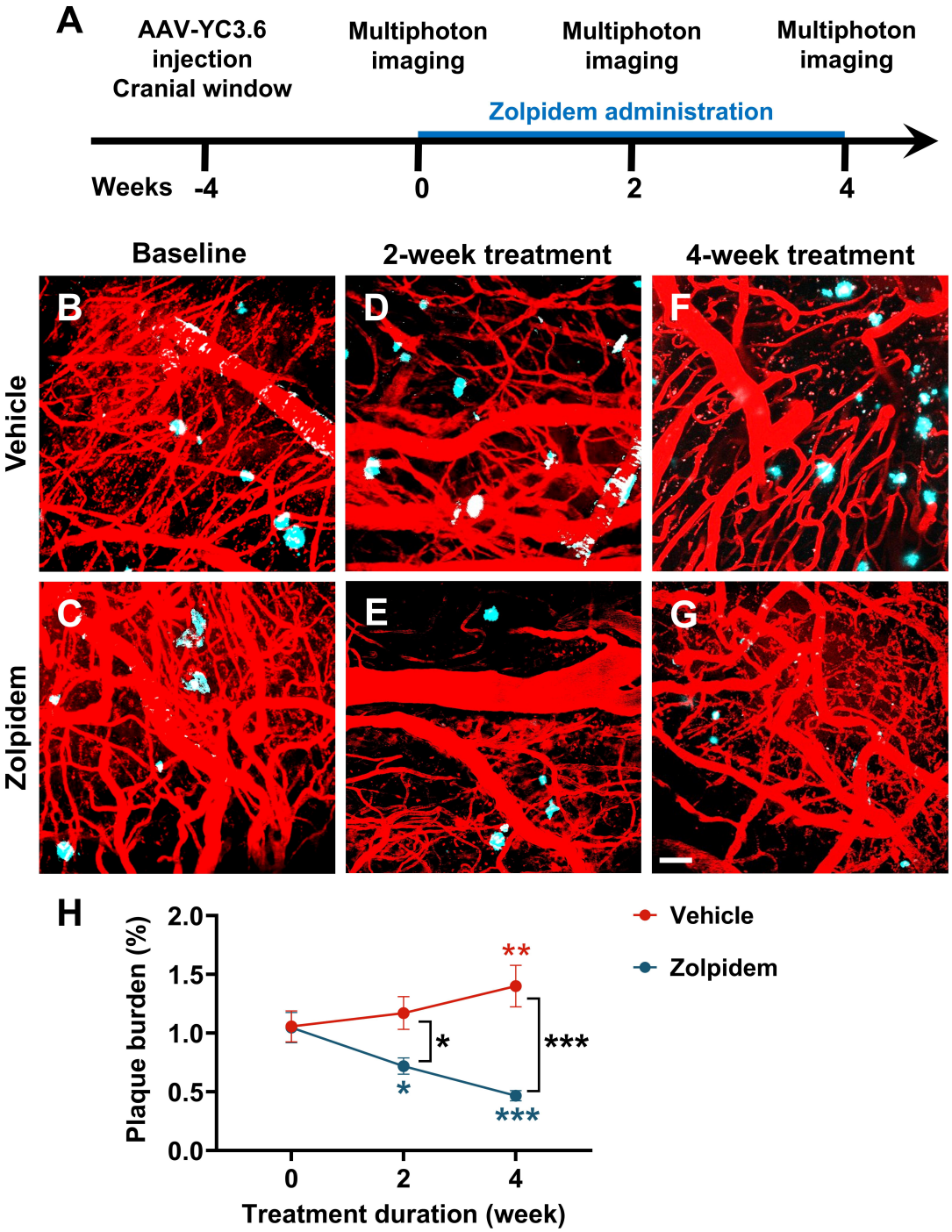
A
AAV-YC3.6 injection Cranial window
Multiphoton imaging
Multiphoton imaging
Multiphoton imaging
Zolpidem administration
Weeks -4
0
2
4
Baseline
2-week treatment
4-week treatment
Vehicle
Zolpidem
B
C
D
E
F
G
H
Plaque burden (%)
2.0
1.5
1.0
0.5
0.0
0
2
4
Treatment duration (week)
**
*
***
*
***
Vehicle
Zolpidem

Figure 6

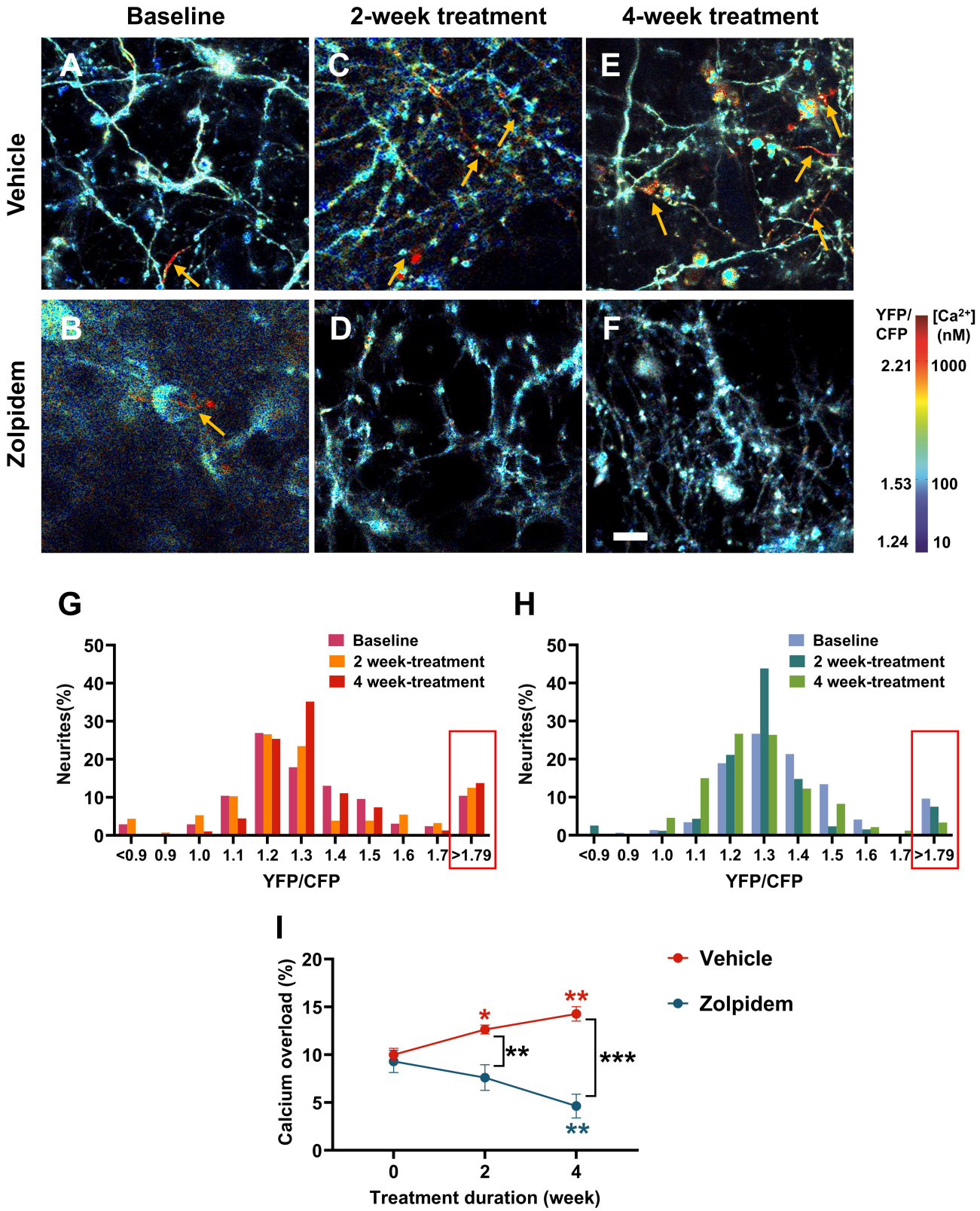
Baseline
2-week treatment
4-week treatment
Vehicle
Zolpidem
A
B
C
D
E
F
YFP/CFP
[Ca2+] (nM)
2.21
1.53
1.24
1000
100
10
G
Baseline
2 week-treatment
4 week-treatment
Neurites(%)
YFP/CFP
<0.9 0.9 1.0 1.1 1.2 1.3 1.4 1.5 1.6 1.7 >1.79
H
I
Vehicle
Zolpidem
Calcium overload (%)
Treatment duration (week)
*
**
***

Figure 7

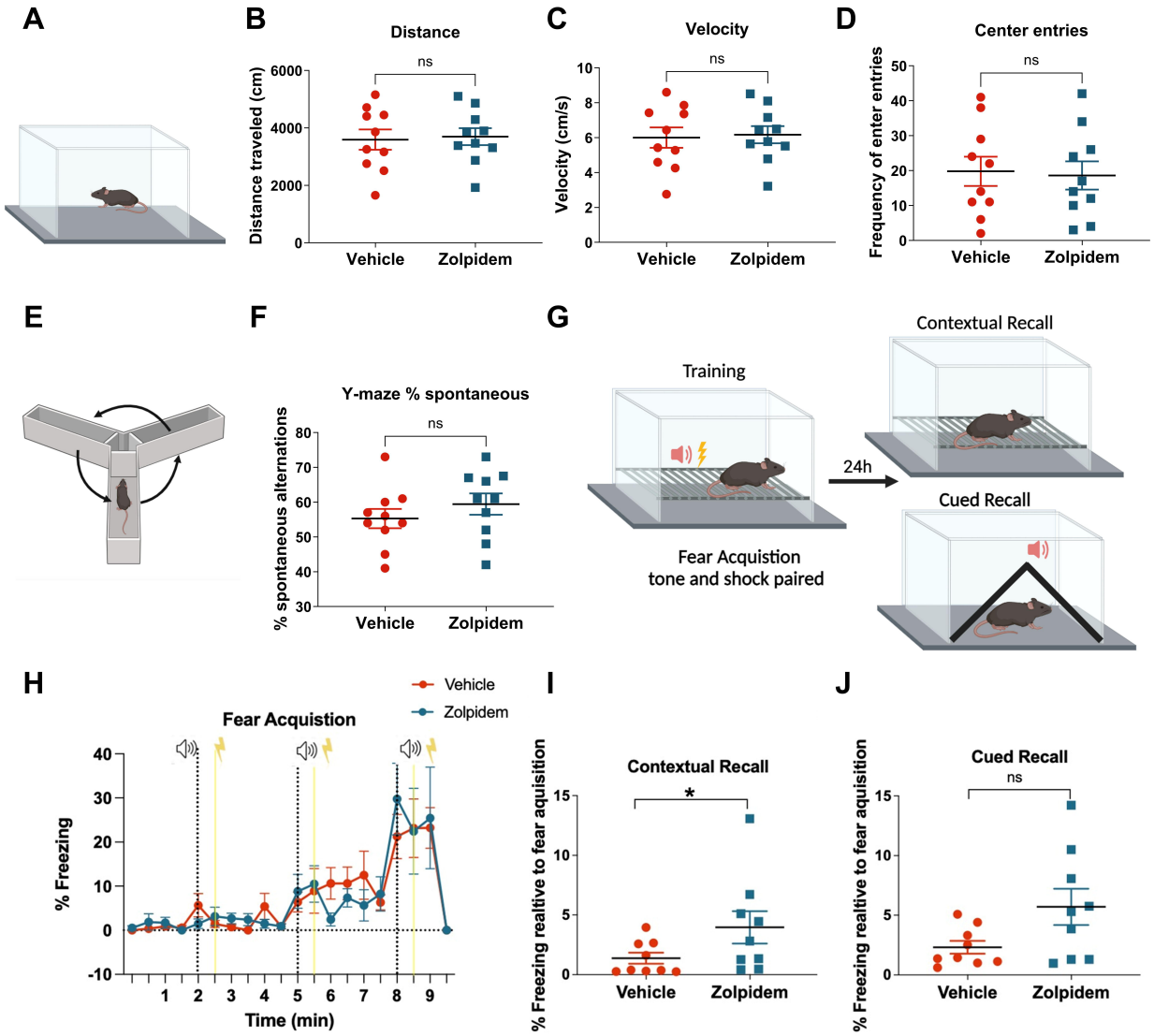
A
B
Distance
ns
Distance traveled (cm)
6000
4000
2000
0
Vehicle
Zolpidem
C
Velocity
ns
Velocity (cm/s)
10
8
6
4
2
0
Vehicle
Zolpidem
D
Center entries
ns
Frequency of enter entries
50
40
30
20
10
0
Vehicle
Zolpidem
E
F
Y-maze % spontaneous
ns
% spontaneous alternations
80
70
60
50
40
30
Vehicle
Zolpidem
G
Training
Fear Acquistion
tone and shock paired
24h
Contextual Recall
Cued Recall
H
Vehicle
Zolpidem
Fear Acquistion
% Freezing
40
30
20
10
0
-10
1
2
3
4
5
6
7
8
9
Time (min)
I
Contextual Recall
*
% Freezing realtive to fear aquisition
15
10
5
0
Vehicle
Zolpidem
J
Cued Recall
ns
% Freezing realtive to fear aquisition
15
10
5
0
Vehicle
Zolpidem